IEEE Access
Multidisciplinary | Rapid Review | Open Access Journal

Received February 16, 2017, accepted April 6, 2017, date of publication April 17, 2017, date of current version June 7, 2017.

Digital Object Identifier 10.1109/ACCESS.2017.2693375

5G Terrestrial Networks: Mobility and Coverage–Solution in Three Dimensions

NICHOLAS P. LAWRENCE[1], BRIAN W.-H. NG[1], (Member, IEEE), HEDLEY J. HANSEN[1,2], (Member, IEEE), DEREK ABBOTT[1], (Fellow IEEE)

[1]School of Electrical and Electronic Engineering, The University of Adelaide, Adelaide, SA 5005, Australia
[2]RFT Group EWRD, DSTG, Edinburgh, SA 5111, Australia

Corresponding author: Nicholas P. Lawrence (nicholas.lawrence@adelaide.edu.au)

ABSTRACT The next generation of wireless communications, which is proposed to operate in the mmWave region of the electromagnetic spectrum, offers the potential of high-data rate and increased coverage in response to a rapid growth of mobile data traffic. Operation in an mmWave channel is subject to physical and current technical limitations compared with conventional terrestrial microwave channel propagation. In this paper, the effects of antenna misalignment are considered in an mmWave channel through polarization mismatch. Tri-orthogonal polarization diversity is suggested as a means for mitigating misalignment effects and offering increased link performance over a majority of antenna orientations. A known physically realized planar antenna design offering such diversity is highlighted.

INDEX TERMS 5G, polarization diversity, Internet of Things.

I. INTRODUCTION TO 5G TERRESTRIAL NETWORKS

The next generation of wireless networks is expected to handle up to a thousand times more traffic than 2013 levels by 2020. Higher operating frequencies in the mmWave region of the electromagnetic spectrum are being considered as a lack of available bandwidth currently is an issue at conventional operating frequencies [1]. The mmWave region extends from 30–300 GHz [2], sitting between the microwave region (3–30 GHz) [2] while overlapping the lower region of terahertz frequencies (100 GHz–30 THz) [3]. The mmWave region is shown in Figure 1, together with frequency bands of interest for the next generation of wireless networks.

As the drive to develop new networks is pursued, a compelling argument exists that wireless radiated energy needs to be used efficiently if designs are to be effective. Networks operating in the microwave region make use of several advantages that may not necessarily exist in the mmWave region. These include:

- high transmit power due to reduced intermodulation and non-linear effects.
- low spreading loss and atmospheric absorption.
- good coverage due to a wider beamwidth.
- multipath fading providing diversity, particularly in dense urban environments.

In the mmWave region of the electromagnetic spectrum, signal propagation is subject to:

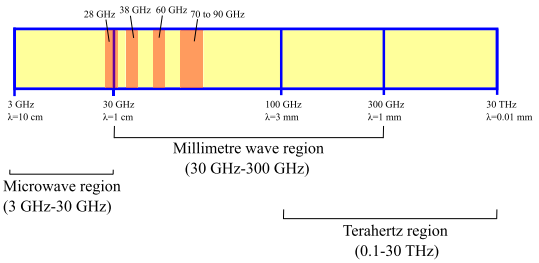

FIGURE 1. The mmWave region of the electromagnetic spectrum. The mmWave region extends over a region of 270 GHz, from 30–300 GHz. Frequency bands of interest for the next generation of wireless networks are shown. Note that there is no standardized definition of the terahertz band. Whilst terahertz spectroscopists loosely define the band as the 0.1 THz to 10 THz range, another common alternative range is 0.1 THz to 30 THz.

- lower transmit power due to increased intermodulation and non-linear effects
- higher spreading loss and atmospheric absorption
- reduced coverage due to a narrow focussed beamwidth
- reduced range resulting from reduced beneficial multipath fading, due to a reduction of scattering mechanisms at higher frequencies and lower transmit power.

Coupled with a lower transmit power due to non-linear effects, a reduced beamwidth at mmWave frequencies, as seen in Figure 2, provides a reduced probabilty of multipath fading. Multipath fading in a rich scattering

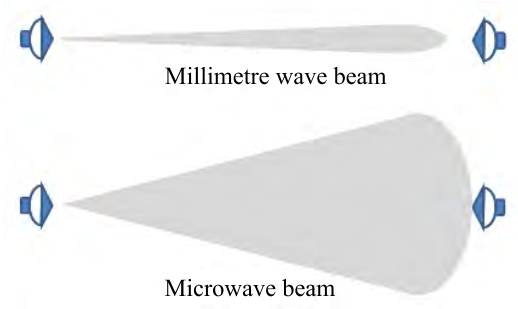

FIGURE 2. Millimetre wave beamwidth. Due to increased free space path loss, mmWave beamwidths are narrow in order to focus radiated energy in the direction of propagation. A consequence of this is a more LoS channel when compared to those operating at microwave frequencies, requiring beam steering of radiated energy. The LoS channel is also typical of satellite channels, which are proposed to be integrated into new fifth generation, or 5G, wireless networks. After [4].

environment typically provides several copies of a propagated signal through a channel, as a consequence of the signal being hived into multiple lower power copies of itself due to scattering effects. This provides several resolvable signals that propagate along distinct subchannel paths to a receiver, increasing the possibility of reception [5]. Broadly speaking, to increase capacity across a channel, narrowband signals should be used in place of wideband or spread spectrum signals, with the number of resolvable signals kept low while providing diversity [6].

A. WHY IS THERE AN ISSUE CURRENTLY FACING WIRELESS NETWORK DESIGN?

Mobile data growth has reached a tipping point. The rapid explosion in wireless services over the past couple of decades has presented numerous challenges and subsequent solutions in order to provide the wireless subscriber with content. Diversity techniques coupled with coding techniques have provided near ubiquitous wireless coverage for all. The introduction of smartphones, enabling various data forms to be transferred wirelessly at the touch of a screen, has revolutionized personal communication. Systems are constantly evolving in order to provide the user with improved content. To provide higher end content to the wireless subscriber, more data is typically required to be transferred. This requires higher data transfer rates, or a wireless subscriber who is willing to wait longer for data to be transferred to them. With the latter option not being credible, data transfer rates must increase. Available bandwidth at operating frequencies used in current systems is limited, and this is driving the next generation of wireless design.

B. WHAT EXACTLY IS BEING DONE ABOUT IT?

Engineers are agreed that higher operating frequencies will be required to advance mobile data growth and expectations. The introduction of fifth generation, or 5G, regulations aims to provide systems that may deliver data transfer rates or capacity two to three orders of magnitude higher than those currently available [1]. To achieve this, we may consider Shannon's theorem on the capacity C of a channel in bits/sec with additive white Gaussian noise,

$$C = B \log_2 \left(1 + \frac{S}{N}\right) \tag{1}$$

where B is the channel bandwidth in Hertz and S and N are the average power of the received signal and noise over the bandwidth in Watts, respectively. In order to provide multi-gigabit/sec data transfer rates, the theorem suggests that the capacity of a channel requires a commensurate large bandwidth and large signal power.

The search for methods to increase data transfer capacity to satisfy future mobile traffic demands stems from an initial decision in December 1995 by the US Federal Communications Commission to allocate a 5 GHz band for unlicensed applications in the mmWave region around 60 GHz. A subsequent modification to this allocation resulted in the band being extended to 7 GHz (57-64 GHz) [7]. Many countries have opted for similar frequency band allocation for high data rate unlicensed communications at mmWave frequencies, and this is shown in Figure 3.

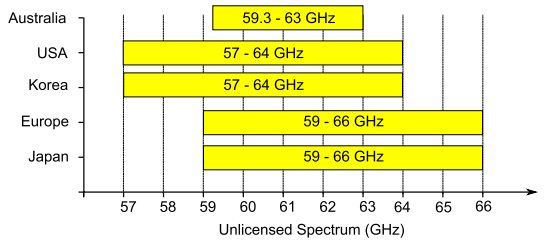

FIGURE 3. In countries around the world, an unlicensed 60 GHz bandwidth exists with a large ultrawide bandwidth, typically of 7 GHz. The allocation of an unlicensed ultrawide bandwidth at 60 GHz, in the mmWave region, has paved the way for exploring the possibility of high capacity data transfer methods for fifth generation, or 5G applications.

At 60 GHz, strong attenuation caused by the resonance of oxygen molecules exists, and so this band is in principle not suitable for long-range wireless communication of the order of a few kilometres. This range limitation permits spectrum reuse by multiple systems within close proximity of one another. Furthermore, as well as a larger available bandwidth at higher frequencies resulting in higher capacity data transfer, operation at mmWave frequencies allows both antenna sizes and spacing in multiple-antenna systems to be reduced. This offers the possibility of compact systems that are affordable [8] and able to be integrated into areas such as textiles [9], potentially offering an unprecedented access to wireless communications.

In many parts of the world, research into 5G technologies is not confined to a single frequency band around 60 GHz. In the UK, a portion of the mmWave region of the electromagnetic spectrum between 28–80 GHz is being investigated [10] to provide an increase in data transfer capacity. In the US, the frequency bands of interest are given below in what is known as the Spectrum Frontiers Proposal [1], [11]–[15]:

TABLE 1. Unlicensed wireless communication bands. A comparison of the different features of some of the in-use license-free wireless communication bands and those at 60 GHz in the mmWave spectrum.

	802.11b	Bluetooth	802.11a	UWB	60 GHz
Cell radius (m)	100	10	50	10	10
Information rate per channel (Mbps)	11	1	54	50	500
Number of channels	3	10	12	6	10
Capacity (Mbps/m^2)	0.001	0.03	0.1	1	16

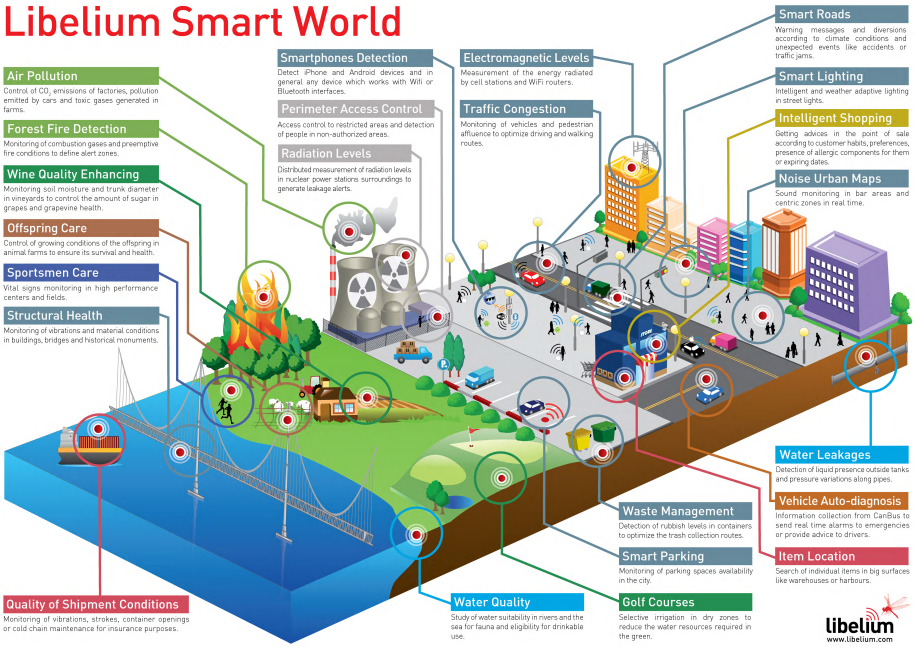

FIGURE 4. A view of the shift towards total wireless connectivity. The next generation of wireless networks aims to offer connectivity to up to a thousand fold more devices, but many questions remain as to how to progress to a target that has been set for 2020. After [25].

- 24 GHz Bands (24.25–24.45 GHz and 25.05–25.25 GHz)
- Local Multipoint Distribution Service Band (27.5–28.35 GHz, 29.1–29.25 GHz, and 31–31.3 GHz)
- 39 GHz Band (38.6–40 GHz)
- 37/42 GHz Bands (37.0–38.6 GHz and 42.0–42.5 GHz)
- 60 GHz Bands (57–64 GHz and 64–71 GHz)
- 70/80 GHz Bands (71–76 GHz and 81–86 GHz).

In the US, interest in increasing data transfer rate was initially placed on technologies operating in the frequency band of 3.55–3.65 GHz, only slightly higher than those conventionally used, as frequencies beyond 24 GHz were perceived as unsuitable for signal propagation due to physical and technical limitations [16]. However, it is now understood that multiple ricochets providing multiple reflections and hence multiple copies of a signal transmitted at 24 GHz or above are available after channel propagation at the receiver [17], [18]. These processes provide diversity. Disparate signals resulting from these processes may be received by MIMO antennas and subsequently built into an intelligible data signal potentially offering multi-gigabit data transfer rates [1], [19].

The allocation of a 7 GHz bandwidth for the next generation or fifth generation of license-free communication devices operating at 60 GHz offers the possibility of enhanced transfer rates. Such data rates are far higher than those encountered at conventional low microwave frequencies [20]. In Table 1, a comparison is made between different features of current in-use license-free wireless communication bands and those in the 60 GHz band.

The move to the mmWave spectrum is in anticipation of up to a thousand fold increase in mobile traffic by 2020. While mobile subscriber numbers are saturated in many developed countries, it is expected that content is likely to increase requiring greater network capacity. This traffic is to be driven primarily by the rapid spread of mobile networks into developing countries, as well as the integration of smart goods on to wireless networks, known as the Internet of Things [21]. To summarize, the rollout of 5G is looking to provide:

- increased coverage [1]
- integration of networks including satellite and terrestrial networks [15], [22], [23], and the Internet of Things [24]–[26].

Proposed concepts of the next generation of wireless interconnectivity are highlighted in Figures 4 and 5.

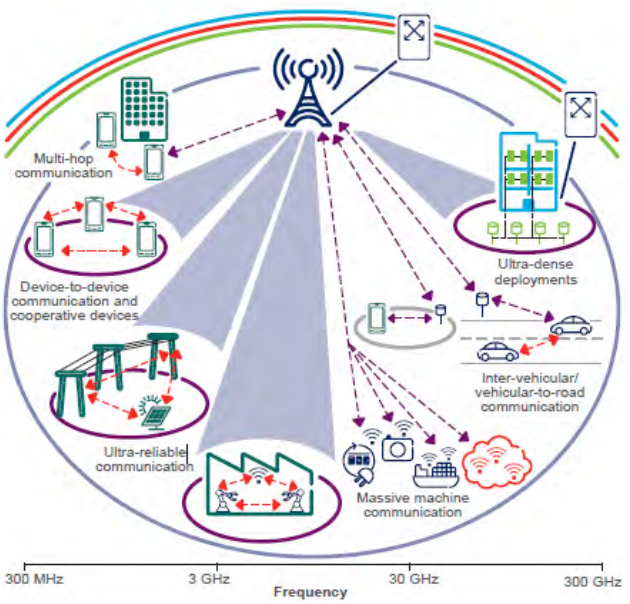

FIGURE 5. Driverless vehicles and remote surgery are offered through wireless total connectivity. Wireless connectivity for all devices offers the possibility of wireless control and optimisation of a majority of household appliances and industrial equipment in what is known as the Internet of Things. After [26].

C. HOW CAN TRI-ORTHOGONAL POLARIZATION DIVERSITY IMPACT THIS ISSUE?

The rollout of 5G is currently little more than a concept, with a fully fledged industry standard yet to be agreed upon. Standardisation of the concept is urgently required. Multiple groups are working on standards regarding interoperability and backward compatibility issues [15], [27], [28].

Improved coverage is one aspect that is targeted in the 5G rollout. This statement is ambiguous as coverage is nominally applied to spatial position alone. If networks are to perform as required, the challenges of operating at mmWave frequencies need to be considered [1]. These challenges are brought about as a consequence of:

- higher transmit power being required to combat free space path loss effects over the channel
- higher transmit and receive antenna directivity being required to focus power, typically along boresight
- nonlinearity and intermodulation effects increasing as a function of frequency, restricting linear power transmission
- smaller component size creating issues for component heatsinking and effective aperture area.

In addition to these challenges, the effect of polarization mismatch, or antenna misalignment, may drastically reduce system performance. To mitigate antenna alignment issues, circular polarization (CP) is used as a *de facto* signal propagation technique [29]. In effect, the transmitted electric vector tip may be considered as rotating about the direction of propagation [30]. As a result, a component of the propagated signal is always received, and for transmit and receive antennas that are perfectly aligned along a direction of propagation a CP wave is received provided that a CP wave is transmitted and that the channel affects the orthogonal linear components of the CP wave in an identical manner.

Deviation of alignment of an antenna at either end of the channel, a transmitted signal with axial ratio that is not 0 dB, or channel effects that affect one linear component of the CP wave more than the other, develop an elliptically polarized (EP) wave. In the extreme case, the EP wave may become linearly polarized (LP), and this may severely degrade link propagation. In [1], the notion of beam steering is highlighted as a solution to misalignment issues.

This article reviews improving coverage through polarization diversity in three orthogonal directions, otherwise known as tri-orthogonality. Diversity offers alternatives signal propagation paths, and in so doing offers link possibilities in channels that would otherwise prove impenetrable. Polarization diversity uses orthogonality of polarizations to provide a compact solution offered in two dimensions [31], [32].

Extending polarization diversity to three orthogonal dimensions effectively provides a colocated solution that theoretically may provide enhanced diversity, and the potential to beam steer to increase radiated electromagnetic energy in any link direction. In so doing, the angular range of coverage is expanded. However, physical antenna solutions no longer remain planar in nature, and acquire volume [33]. Therefore, compactness of the solution is hitherto unavailable.

In [34], a tripling of capacity is suggested for a tri-polarized orthogonal arrangement at the antenna. The experiment is conducted at a frequency and in a context that produces a rich scattering environment. In effect, this does not provide a full picture of the tri-orthogonal arrangement as misalignment issues are mitigated by such an environment. A similar environment is presented in [33].

With these issues raised, the paper aims to provide the following:

- a review of the effects of misalignment and its mitigation by a tri-orthogonal antenna arrangement over a range of channel environments
- a brief review, with pointers to the literature, on a recent tri-orthogonal polarization diverse antenna solution.

D. MOTIVATIONS AND OBJECTIVES

Wireless subscribers are predominantly concerned with ubiquitous, ever increasing amounts of content. In order to provide this, data rate needs to be consistently augmented. At this point in time, conventional wireless propagation techniques have been more than adequate providers of content. Systems have made the best use of a signal wavelength which is often longer than objects found in the channel environment. Propagated signals have been able to reflect from and refract around objects to provide reception in places where no LoS signal propagation is possible.

Strong reception signals have been a direct consequence of multipath fading effects. Where deadspots have occurred where no reception is possible, be it as a result of signal blockage or superpositioned cancellation of signals at the

receiver, a solution has been to add an additional transmit antenna. At the terrestrial level, and in an environment where it makes economic sense to do so, the policy of transmit spatial diversity has been extremely useful.

Furthermore, to increase rate, and so provide greater content, signal processing methods have been able to code signals to increase rate. Higher levels of complexity in coding typically rely on higher signal-to-noise ratios. Wireless network systems' architects have been able to squeeze as much rate as possible out of conventional networks. In environments where it is not economically viable to perform such measures, or in environments where it is just not feasible to do so, content has not evolved to the same extent.

The growth of mobile data in recent years has now reached a point where it has saturated networks. Additional bandwidth is required if this growth is to continue. But there is also a need to make systems more efficient if we are to reap the benefits of the next generation of wireless design.

When engineers highlight data rate, several points need to be made. Firstly, a maximum rate is often quoted [35]. Secondly, the conditions in which network performance is measured may be optimal [36]. Like-for-like comparisons become difficult. Thirdly, perfect antenna alignment of transmitter and receiver is the norm. After all, what would be the point of measuring rate using a misaligned system. Crucially, the third of these points is very much in focus if 5G is to deliver on what it promises.

The concept of ubiquitous coverage has been mentioned as a goal of the rollout 5G networks. The definition remains rather vague, however. Coverage as a function of spatial positioning of antennas and as a function of relative angular alignment of antennas are not the same, and it can be argued that the latter is of more relevance as engineers look to use radiated power efficiently [1].

This paper considers a definition of coverage in terms of antenna alignment. A misalignment of incoming electromagnetic signal and receive antenna reduces link performance, and in the most extreme case may render the link inoperable. Figure 6 highlights the effect of polarization misalignment. For terrestrial wireless systems, polarization is defined by the orientation of the electric field vector relative to the plane of the Earth.

Polarization mismatch is typically observed as a signal drop at the receiver due to a misalignment of electric field vectors of an incoming signal and of the receive antenna. The misalignment may result from incorrect alignment of the transmit antenna with respect to the receive antenna to begin with, or the propagating signal experiencing depolarizing effects in the channel, or a combination of both.

Conventional techniques to combat such issues have included an increase of power at the transmitter, spatial diversity through provision of additional antennas spaced apart from each other, and signal propagation using circular polarization techniques. In the latter, a component of the rotating electric vector tip of a propagating waveform is always received. However, a circularly polarized waveform

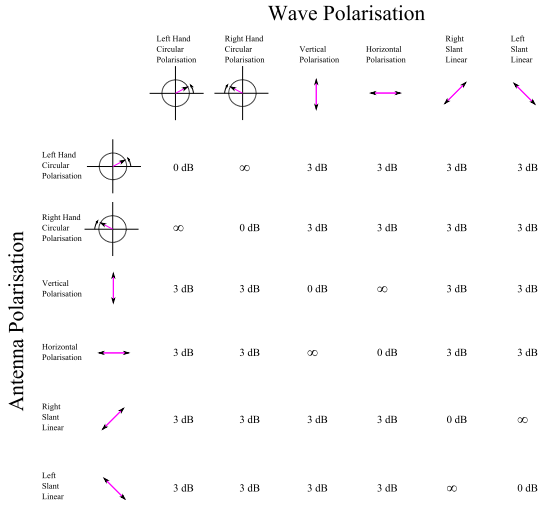

FIGURE 6. The various possibilities of polarization misalignment and subsequent mismatch loss. polarization is defined by the orientation of the electric field vector relative to the plane of the Earth. The effect of polarization misalignment between an incoming electromagnetic signal and a receive antena may render links inoperable in the most extreme cases.

may only be transmitted in one direction, and any deviation of a receiver away from this direction typically results in elliptically polarized reception.

In the extreme case, reception may become linearly polarized that may result in a drop in system capacity. Deviation from a case of perfect reception of a circularly polarized waveform may be exacerbated when the effects of specular reflections and multipath are also considered. Specular reflections of a signal provide a 180° shift in phase between propagating vertical and horizontal components of a circularly polarized signal. In an extreme case, a right handed circularly polarized network may provide no reception at the receiver as the signal has become left handed circularly polarized as a result of such a reflection.

In the instance of multipath fading, received signal components may effectively cancel each other out at the receiver, providing reduced range or spatial positions of impaired or indeed no reception. Such fading may affect reception of a signal with purely LoS components, or that with stochastic components introduced through propagation over the channel. Signal scatterers may scatter a signal to the extent that all resulting diverse signal components are too weak for reception. The benefit of multipath is dependent on a high SNR at the receiver, together with a limited cancellation effect of superpositioned received signal components. These components provide diversity at the receiver as a result of propagating along uncorrelated individual subchannel paths.

With increasing path loss, or reduced transmit power, multipath effects degrade signal reception more readily, as received signal strength begins to fall consistently below the receiver noise floor. The ability to provide an increased signal strength at the receiver becomes crucial in mitigating specular reflective effects and in providing beneficial multipath fading effects.

Fifth generation or 5G networks are looking to provide greater content in a unit time period through higher operating frequencies in the mmWave region of the electromagnetic spectrum. With new horizons appear new issues:

- higher operating frequencies are subject to increased free space path or spreading loss due to a smaller wavelength of operation [37]
- signal absorption at higher operating frequencies is higher than that encountered at conventional terrestrial network operating frequencies [38]
- mmWave signals are not scattered to the same extent as conventional high power low gigahertz signals, as narrow beamwidths are required to focus transmit power. Multipath effects are typically not as beneficial [39]. Instead, a LoS signal tends to dominate. All of this suggests a higher power requirement
- higher power amplifiers at mmWave operating frequencies are typically inefficient smaller devices than those at low gigahertz frequencies [8]. Inefficiency leads to increased heat energy that must be dissipated effectively
- as operating frequency increases, solid state power devices typically become less efficient and are subject to non-linear effects [40]. Third order intermodulation, where an unwanted signal becomes dominant in an operating bandwidth, restricts transmit power. While not necessarily a problem in a terrestrial environment at the transmitter, where power amplifiers may be banked together to provide the required output power without producing an unwanted third order intermodulated signal, it is indeed a problem for a mobile handheld receiver where mass and volume are restricted. The same criteria equally applies to a satellite payload providing communications coverage to thousands of subscribers.

For static systems, such as a fixed point-to-point terrestrial network or geostationary satellite providing a service within a fixed field of view, the alignment issue can be managed to provide adequate gain and power to subscribers. We however live in a mobile world, and so for subscribers to terrestrial networks using handheld devices, and for subscribers to satellite services where global coverage is proposed, requiring satellites that move relative to the Earth's surface, the issue of alignment becomes crucial.

One of the aims of 5G is to combine terrestrial and satellite services to improve coverage [22], [23], and this will require consideration of efficient antenna design. In this context, conventional techniques are no longer adequate. We need to think in three dimensions, and to provide mechanisms in which we may efficiently radiate electromagentic energy through compact design.

Diversity, or the ability to provide additional paths of signal propagation is possible in many forms. If space is no problem, spatial diversity, such as telecommunications providers use in urban centers where antennas are placed on numerous rooftops to provide maximum coverage, is considered as a conventional solution. When space is constrained,

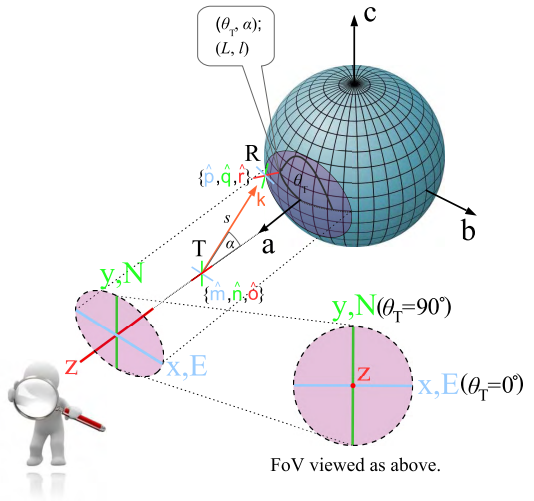

FIGURE 7. Frames of reference. In this paper, a field-of-view (FoV) is seen from the perspective of the transmitter T, with the receiver R moving over the sphere, covering all antenna orientations. The nomenclature in this figure is used throughout this article.

one technique of providing additional diversity is through polarization.

Tri-orthogonal polarization diversity exploits radiated electromagnetic energy in three orthogonal directions to provide enhanced link performance. Prior research in this field has typically been demonstrated in environments that facilitate propagation [33], [34]. In effect, a rich scattering environment provides the possibility for an arbitrarily polarized signal to be transmitted and subsequently received. This is fine in such an environment, but what about in channels that are not rich scattering environments?

Rich scattering environments may not necessarily exist in a 5G terrestrial mmWave channel, or in a satellite channel. Satellite channels are proposed to be included in the next generation of wireless communication in order to improve coverage. In both, a LoS signal may typically dominate. Add movement of the receiver relative to the transmitter into the mix, and angle of transmission and reception become critical in the ability to propagate a signal.

In this section, we have introduced the issues regarding the next generation of wireless communication. These issues are poignant, given the timeline that is required to be followed if the growth in mobile data is to continue. Suggestions are proposed with regard to the role that the research undertaken in this article might play in helping to solve these issues.

In Subsection II-A, a review is undertaken of tri-orthogonal polarization diverse methods applied to terrestrial design. As one of the aims of 5G is to provide improved wireless coverage, including through interconnection of terrestrial and satellite systems, a critique of channel modeling is presented in Subsection II-B. This critique provides a basis for a channel model that considers tri-orthogonal polarization diversity applied to a terrestrial channel that is presented in Section III.

In Section III, and through a metric of system capacity, operation in a terrestrial channel of a link operating

at 60 GHz, in which tri-orthogonal polarization diversity at both transmitter and receiver is provided, is considered. Simulation of a AWGN fading channel where only a line-of-sight signal exists is performed, along with that of a Rayleigh fading channel. Both simulations are conducted over a transmit field-of-view covering all possible orientations at the receiver.

The simulations suggest that in a AWGN fading channel, the tri-orthogonal system provides orientation robustness above that of a conventional dual polarized system, while in a Rayleigh fading channel, capacity is significantly increased over the majority of the FoV.

Simulations cover extreme channel conditions in both cases, and suggest that a tri-orthogonal approach is beneficial in both cases. Ideally, we would once again want capacity to be independent of propagation angle, and tri-orthogonal polarization diversity is shown through a fundamental physical approach to provide an improvement in this respect.

II. MISALIGNMENT MITIGATION THROUGH TRI-ORTHOGONAL POLARIZATION DIVERSITY

Polarization diversity offers the possibility of transmitting distinctly polarized signals that may be subjected to individual subchannel path effects. At mmWave operating frequencies where signals may be more line of sight due to narrow beamwidths, such an arrangement provides diversity and resolvable signals at the receiver. A similar argument holds for satellite channels, which are typically LoS in nature, and are proposed to be integrated into new fifth generation, or 5G, networks [22], [23], [41], [42].

A. TRI-ORTHOGONAL POLARIZATION DIVERSITY REVIEW

The concept of tri-orthogonal polarization diversity is most prominently highlighted in [34], where the concept of tripling capacity using a colocated orthogonal arrangement of antennas is demonstrated under laboratory conditions at an operating frequency of 880 MHz. The use of a mirror provides a method of generating mutiple reflections, simulating the conditions of a rich scattering environment, as found in urban environments for example.

The paper makes the claim that a tripling of capacity is made in such an environment over a DP radio signal, as three electric and three magnetic polarized states are present. The concept delivers a channel of rank six, suggesting that all states are contributing to system capacity as all eigenvalues are non zero and distinct. This rank suggests a three fold increase over a DP electric signal with no scattering.

Figure 8 illustrates the experimental arrangement. The orthogonality of the MIMO system provides a low mutual coupling value of -25 dB between polarized states. Each antenna associated with a polarized state provides an omnidirectional radiation pattern with nulls of -25 dB parallel to the antenna axis at the operating frequency used.

The proximity of experiment and theory is seen in the capacities of Figure 8. Theoretical studies on this arrangement have also highlighted the use of three electric and three magnetic polarized states, and the implications for enhanced channel capacity [43], [44].

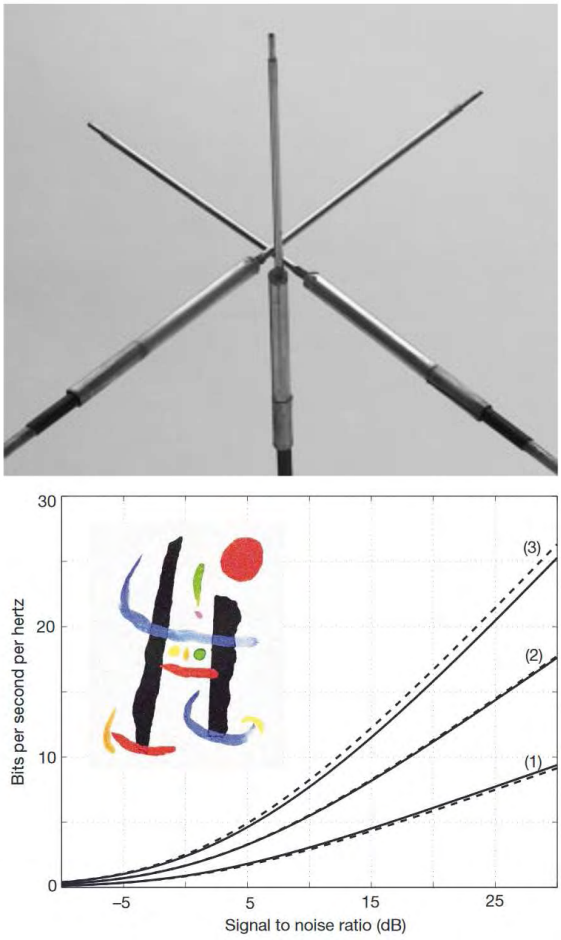

FIGURE 8. Colocated tri-orthogonal antenna arrangement. Capacity measurements made for one (1), two (2) and three (3) orthogonal antennas are shown by solid lines. Random matrix channel theory solutions are shown for the same arrangements by the dotted lines. A tripling of capacity over the rich scattering channel is observed for the case of the tri-orthogonal arrangement. The colour image, ***A toute épreuve*** by Joan Miro, is reconstructed from transmission of three distinct red, green, and blue monochrome subfields on each of the three orthogonally oriented antennas observed in the upper portion of the image. After [34].

In [44], electric current and magnetic current profiles generate six polarization states and are analysed by ideal point sensors, providing a theoretical six-fold increase in capacity. Practical antennas are of finite size, however, and transmit and receive topologies of electric half-wave dipoles and magnetic full-wave loops are also analysed. In a rich scattering multipath environment, all six polarization states are found to be uncorrelated and of equal strength. The magnetic states are not found to contain any additional information than that of the electric states, and as such are redundant. In addition, the radiation patterns are found to interfere, and become non-orthogonal. As such, no more than three orthogonal electric polarization states are suggested as useful for a tri-orthogonal arrangement.

In [45], the effect of mutual coupling on capacity is explored. The effect is considered for the case of two radiating elements that begin as widely spaced apart, but that are systematically brought closer together.

The mutual coupling effect is of interest as it is observed that capacity is observed to increase in the instance of close spacing, which is counter to the understanding of mutual coupling impinging on capacity. As the radiating elements combine to form one element, capacity drops commensurately. The effect of mutual coupling is interesting for a tri-orthogonal arrangement in as much as such an arrangement consists of antennas that are already in close proximity, and that mutual coupling is being mitigated by the orthogonal nature of the arrangement. Indeed, a certain amount of confusion surrounds the effect of mutual coupling on capacity as suggested by the contradictory stances of [46] and of [47]. Whereas the former suggests the negative consequences of mutual coupling, the latter suggests that some amount of mutual coupling is useful.

From a classical standpoint, capacity may be construed as received power. As such, a certain amount of mutual coupling is beneficial in the sense that received signal power is coupled to antennas that are in close proximity to each other; the point that is made in [45].

However, mutual coupling affects pattern diversity, resulting in static asymmetric patterns that are unusable for providing an option to beam steer, or an option to differentiate link directions. Whereas a poorly defined radiation pattern is common in mobile phone, or planar inverted-F, antennas (PIFAs) [48]–[50], this is mitigated by high power transmission from base stations. For higher operating frequencies, and LoS applications, this form of mitigation does not exist.

In [43], a four fold limit on capacity enhancement is placed on an array of planar antennas compared to a LP array. In effect, only four of the tri-orthogonal polarization states are used, two electric and two magnetic states. A volume array, or arrangement of tri-orthogonal antennas, gives an additional logarithmic increase in capacity. This may be understood by the redundancy of two polarization states in a direction of propagation along an antenna axis. However, it is the ability of the tri-orthogonal arrangement to compensate a loss of capacity on a pair of electric and magnetic polarization states with an increase in capacity for the orthogonal polarization states, in effect providing a quasi-isotropic solution and mitigating antenna misalignment, that is of interest.

In [51], a colocated tri-orthogonal arrangement at both transmitter and receiver is demonstrated in an indoor environment at 2.44 GHz. Experimental results suggest that the arrangement is suitable for high capacity mobile systems. The authors suggest that there is degradation of capacity in as a function of elevation but not as a function of azimuth. Whereas there may be an issue regarding non-orthogonality of radiation patterns due to an effect of mutual coupling between radiation patterns in one direction and not the other, the difference in capacity performance as a function of angle is small.

In [52], a tri-orthogonal arrangement of UWB antennas is investigated. However, the experiment does not use a colocated arrangement, as it is conducted according to the method of [53]. As such, the beneficial effects of spatial diversity and reduced mutual coupling are included, and so the experiment does provide an exaggerated account of the performance of the tri-orthogonal arrangement.

The MIMO cube of [54] is an interesting concept, highlighting the orthogonal and symmetric nature of tri-orthogonality through a cubic arrangement with the possibility of 12 distinct radiating elements, providing 12 subchannel paths or eigenmodes. In the work of [54], for a half-wave dipole length of side and in a Rayleigh rich scattering channel, a theoretical capacity increase commensurate with the number of active eigenmodes is seen compared to LP polarization state transmission. However, this capacity enhancement is observed to decrease as the side of cube is decreased, rendering the design impractical for mobile applications.

In addition, the effects or mutual coupling and reduction of pattern diversity of not considered. Mutual coupling reduces capacity performance of close proximity radiating elements [46]. In [55], the effect on the MIMO cube is theoretically scrutinized, and it is suggested that mutual coupling reduces capacity only for cubes of length of side less than 1/3 of a wavelength. In effect, mutual coupling acts to limit antenna compactness.

A physical version of the MIMO cube, presented as a slot radiator rather than dipole radiator, is provided in [56]. This is shown in Figure 9. The design is observed to suffer from the effects of mutual coupling, and this in turn effects polarization diversity through polarization impurity which in turn affects pattern diversity. The design is elaborated through a series of internal polygon stuctures designed to reduce internal mutual coupling effects, and this in turn reduces mutual coupling by 20 dB, and improves the radiated patterns of the slots.

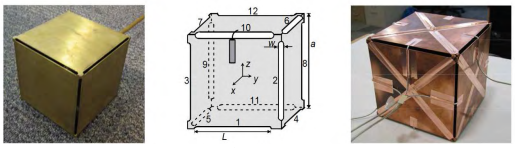

FIGURE 9. Slot radiator version of the MIMO cube. The images shown are: (a) original version, (b) hollow cube schematic, (c) second version where by internal polygon structures are included to reduce mutual coupling effects. After [56].

A tri-orthogonal antenna design using FR4 dielectric material is demonstrated in [33], operating at 2.55 GHz. Figure 10 presents the design. The design provides 18 dB of polarization isolation between antennas. Radiation patterns are somewhat affected by this small degree of polarization impurity, and the material and structure of the design itself, which is slotted together to provide a polarization orthogonal to a typical planar surface.

The design in [33] is tested and shown to provide a tripling of capacity in a rich scattering Rayleigh fading channel.

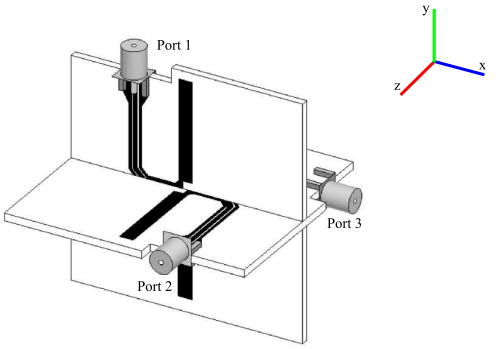

FIGURE 10. A tri-orthogonal antenna constructed using FR4 material. The tri-orthogonal design is slotted together to provide a third polarization orthogonal to the planar *xz* surface, which is excited by port 1. After [33].

At the transmitter, spatial diversity exists as the orthogonal radiating elements are not colocated. In addition, the transmitter is descibed as a linear arrangement of antennas, and it is not clear if these are all polarized in the same direction, or orthogonally, as is desired. At the receiver, orthogonally polarized antenna elements are colocated and so spatial diversity is minimized thereby demonstrating the benefits of polarization diversity at the receiver.

The effect of mutual coupling on radiation patterns is mitigated through matched termination of untested ports. An ideal capacity measurement is hence generated, as it is likely that pattern diversity would be affected if all three ports were excited simultaneously, as mutual coupling is −18 dB.

In essence, the designs and analysis given above provide the background to more recent research. A design based on a tri-orthogonal arrangement may be found in [57]. The publication demonstrates a compact tri-orthogonal arrangement using a cross-shaped dielectric resonator antenna (DRA), and operating at 4.7 GHz with a 6.8% overlapping bandwidth. The design is shown in Figure 11. Mutual coupling is kept below −30 dB by a symmetrical and orthogonal design. As a consequence, pattern diversity is maintained.

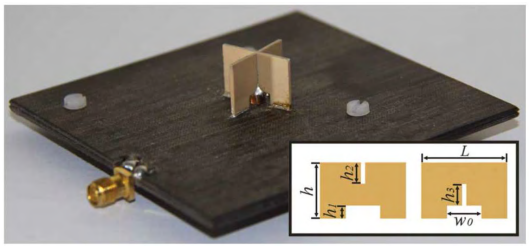

FIGURE 11. A cross-shaped dielectric resonator antenna (DRA) structure, operating at 4.7 GHz with a 6.8% overlapping bandwidth. Low mutual coupling of −30 dB due to the orthogonality and symmetry of the design is recorded for this design. After [57].

To summarize, prior research in this area has conceptually presented tri-orthogonal polarization diversity through theoretical analysis. The following points are noted:

- a tripling of capacity is provided over a LP polarization state in a rich scattering environment, such as a random Rayleigh fading channel. This supports anticipated capacity improvement.
- antenna designs using a tri-orthogonally diverse approach operate at RF and microwave frequencies, conducive to beneficial multipath fading.
- although three magnetic polarization states are also available for channel propagation, there is no additional information that is conveyed by these magnetic states that may not be found in the three electric polarization states. As such, their inclusion is suggested as unwarranted.
- whereas an ideal sensing analysis is presented at the receiver, in practice the implementation of half-wave electric dipoles and full wave magnetic loops is impractical.
- analysis over all antenna directions is not given, and as such results and conclusions are somewhat limited.

In terms of physical design and experimentation, the following points are noted from the results of prior research:

- experimental results of capacity under rich scattering conditions largely match those calculated theoretically.
- a tripling of capacity is provided over a LP polarization state in a rich scattering environment, such as a random Rayleigh fading channel. This bolsters claims of capacity improvement as this tripling may not necessarily be observed for all antenna orientations, and will not be the case for LoS conditions.
- spatial diversity is inadvertently included, and as a consequence mutual coupling effects are largely mitigated.
- mutual coupling effects are reduced through load termination of untested ports. When included, these effects affect pattern diversity.
- mutual coupling effects increase as antenna size is reduced.
- the inclusion of a third orthogonal polarization turns a planar antenna design into a volume antenna design, which compromises the design for mobile devices.
- diversity performance is often erroneously presented, as performance should take radiation pattern weighting into account over an entire radiating FoV.

From this summary, two points are identified to now address:

- what is the enhancement in performance offered by a tri-orthogonal arrangement over all antenna orientations, and over a range of wireless terrestrial channel effects? Moreover, satellite systems are proposed to be integrated into the next generation of wireless terrestrial mobile systems [22], [23], and the concept of tri-orthogonal polarization diversity can be considered in a channel with a time-varying link geometry
- tri-orthogonal arrangements provide a polarization orthogonal to the antenna surface at the expense of a planar design, that consequently becomes a volume design [33], [54]. Can three orthogonal polarizations be provided in a planar design?

Both of these points are important if the next generation of wireless design is to provide higher capacity and mobility while not ignoring fundamental contstraints imposed on current technologies.

B. CRITIQUE OF APPLICABLE MODELING TECHNIQUES

Throughout this article, we highlight the enhancement of wireless communication through tri-orthogonal polarization diversity. This is shown through parameter extremes over a range of channels. The channels have been chosen due to their interest with regard to the next generation of wireless mobile communications, which aims to seamlessly integrate wireless terrestrial and satellite systems [22], [23]. As systems become more mobile, the effect of misalignment becomes more pertinent to performance through polarization misalignment issues, and mitigation is suggested through a tri-orthogonal arrangement.

We present system capacity data according to movement of a receive antenna over a sphere, as a means of analysing misalignment between transmitter and receiver. Studies of capacity performance, including that of MIMO transmission schemes, are typically presented in two dimensional line graph format [58], [59]. Where inference is made to a particular angular orientation of an antenna, the line graph format is maintained [32]. As tri-orthogonal polarization diversity considers three dimensions, so a format encompassing all antenna orientations is required. In this article, capacity performance is displayed for all receive antenna orientations using a convenient circular two dimensional format, or FoV approach.

Furthermore, and by extension, movement of a receive antenna over a sphere naturally lends itself to a non-geosynchronous satellite channel analysis [60], made relevant by the proposed inclusion of satellite systems in the next generation of wireless networks. Combined with a vectorized approach for both wireless terrestrial and satellite channels, three dimensional data is thus able to be presented in a convenient circular two dimensional or FoV format for both systems.

From a terrestrial wireless channel perspective, we acknowledge that channel models are accessible in the literature. However, we suggest that shortcomings are evident in these models:

- models for dual-polarization diverse links make an implicit assumption that perfect alignment exists between transmit and receive antennas, or introduce cross-polar correlations independent of link geometry [61]–[65]
- where performance according to angular orientation is assessed, a two dimensional line graph format considering selected angular orientations is chosen [32]
- where three-dimensional approaches to modeling are observed, research may not consider a tri-orthogonal system [66]–[68]
- a full appreciation of system performance over all antenna orientations in a FoV is typically not presented [69]
- systems are shown that typically operate at frequencies where the effects of rich scattering environments may enhance performance considerably [70]–[72].

The terrestrial model demonstrated in this article provides an initial consideration into the introduction of a proposed mmWave tri-orthogonal system. The tri-orthogonal arrangement offers the potential of short range, high capacity communication, less dependency on spatial position than conventional techniques, and application to all antenna orientations. The simulated results suggest that capacity improvement due to a tri-orthogonal approach is available, both in the presence and absence of channel scatterers. We suggest that our model provides a useful contribution in addition to previous research cited above.

In this section, the reader has been introduced to tri-orthogonal polarization diversity as a possible solution to antenna misalignment. A review of tri-orthogonal polarization diversity is given. The review considers prior research on the topic, both from a system capacity perspective and a hardware design perspective.

A critique of modeling techniques is subsequently presented that considers prior modeling of terrestrial systems, and the limitations of this modeling.

In Section III, tri-orthogonal polarization diversity is applied to a terrestrial 5G channel. All antenna orientations are considered, as a solution to antenna alignment mitigation is sought.

III. APPLICATION OF TRI-ORTHOGONAL POLARIZATION DIVERSITY TO TERRESTRIAL 5G CHANNEL

An era of rapid expansion in consumer wireless applications is forcing demand for additional user capacity, reliability and throughput. One has only to consider the Internet of Things [73], dedicated short-range communications (DSRC) [74] including vehicle-to vehicle technology (v2v) [75], and fifth generation (5G) wireless connectivity [1], [34] to understand that telecommunications are indeed undergoing a marked transformation.

In this new era, the function of wireless technology necessitates consistency, regardless of end user position and orientation. Multiple-input multiple-output (MIMO) signalling techniques have been widely embraced in wireless terrestrial systems, increasing performance by exploiting spatial diversity in a terrestrial channel [5], [76]–[78]. Signal processing theory has primarily considered spatial MIMO applied to LP mode networks [79]–[83], as this has been driven by commercial interests where one polarization is typically transmitted.

At first, polarization diversity did not receive as much attention as spatial diversity. A marked mean signal level difference between co-polarized and cross-polarized branches where one polarization is transmitted is often cited as a reason for this lack of interest [84], driven once again by commercial reasoning. There seemed no reason in providing an additional polarization for little commercial benefit.

A measure of this difference, known as cross polarization discrimination or XPD, is shown at historic terrestrial

network operating frequencies to be typically between 6-20 dB for a given system [31], [85], rising to higher values in suburban than in urban environments, due to a reduced scattering mechanism. The XPD is shown to be correspondingly higher in outdoor than in indoor environments [86], essentially for the same reason.

One advantage of a polarization diverse method over a spatially diverse method is that antenna design may shrink, while providing a comparable, if not superior, performance [61]–[63], [87]. Many CP mode patch antennas designed for operation using CP mode wave propagation demonstrate the case, as these antennas provide superior performance to their LP mode counterparts. Propagation involving a CP mode wave may be decomposed into two orthogonal LP propagation modes with a 90° phase shift between them. For a CP mode receive antenna, loss of reception on one antenna branch or element is mitigated by an increase in reception on the orthogonal branch, providing depolarization mitigation.

The use of a propagating CP mode wave as opposed to a LP mode wave is typically at the expense of a reduced range. For a terrestrial telecommunications operator, range is often the most critical design criteria and, as a consequence, LP mode systems are typically used. A system using CP mode wave propagation and CP mode patch antennas is intended to mitigate depolarization issues [30], and maintains optimum performance as long as antenna alignment exists. The introduction of misalignment reduces performance.

Measurement studies of terrestrial DP diversity involving translation and rotation of a second antenna polarization or branch suggest low correlation and mutual coupling, with MIMO performance superior to that of a spatially diverse system due to the orthogonal nature of the design [31], [32].

In an ideal antenna design, the effects of mutual coupling of antenna polarizations [88] and correlation of antenna polarizations [32] should be mitigated to fully capture the benefit of polarization and pattern diversity [45], [58]. In effect, antenna polarizations or branches should act in an independent yet complementary manner. Additional studies of systems complementing what may be deemed to be spatially polarized diversity measurement, making use of the DP mode technique but not in a unique colocated position, suggest that superior system performance is indeed possible due to low mutual antenna interaction and low correlation [84], [89]–[92].

Currently employed terrestrial systems utilize LP mode or DP mode signal propagation due to their ease of implementation. A comparison of spatial, pattern, and polarization diversity [87] over a range of channel environments suggests that polarization diversity provides 12 dB or more of improvement in SNR; intuitively, a drop in signal on one polarization is compensated for by an increase on another polarization orthogonally colocated.

Antenna interaction and asymmetric antenna patterns in the instance of closely located spatially diverse systems provide an additional argument for the use of polarization diversity, where these two issues may be mitigated through design. Pattern diversity is also feasible for a polarization diverse system, where low gain near-omnidirectional patterns are employed [57].

From a simple geometrical analysis, performance of LP mode, DP mode, and CP mode methods is observed as being dependent on relative antenna positions. These forms of polarization do not consider three dimensional link geometry, instead remaining dependent on ideal antenna alignment. As operating frequency increases in order to provide higher data transfer rates, so consistency of linear transmit power is typically less obtainable at these higher frequencies. Add in a typical reduction of the benefits of multipath fading at the receiver, and the consequence of higher frequency operation is reduced performance, or an exponential rise in system cost to correct this. Orientation robustness, or an ability to maintain performance regardless of device orientation, becomes critical. Every possible design advantage needs to be sought.

For conventional frequencies operated in the RF and low microwave region by mobile wireless operators, networks typically benefit from a rich scattering environment. At these frequencies, operators are typically restricted to increasingly complex processing techniques if they are to provide for a consumer demand of increasing capacity.

Recently, the terahertz region has captured the imagination as high data rates, provided by an unallocated portion of spectrum, offer a multitude of wireless possibilities [93]–[95]. However, wireless operation at terahertz frequencies, as opposed to that at RF and microwave frequencies, has been subject to a slow expansion due to reduced available transmit power, ultimately resulting in propagation in a line of sight (LoS) channel typically devoid of useful scattering mechanisms. As a result, terahertz wireless operation is not yet able to provide orientation robustness to an increasingly mobile end user. Where LoS propagation is disrupted, steerable dielectric mirrors have been introduced [96]. For optical uplink systems to satellites, the effect of beam wander is significantly detrimental to the BER [97].

Novel design at mmWave frequencies offers the potential of many of the advantages to be found at both microwave and terahertz frequencies while reducing the impact of the disadvantages [96]. Primarily, a large 7 GHz bandwidth at 60 GHz, within the mmWave spectrum, has been offered to wireless operation over short terrestrial distances [11]. This offering supports increased rate through the use of less complex modulation techniques, including binary phase shift keying (BPSK). Secondly, design and application may be positively affected by well understood RF and microwave concepts. Thirdly, in the mmWave region, the availability of transmit power does not necessarily constrain the system to LoS propagation. As a consequence, readily manufacturable omnidirectional antenna designs may be used at the transmitter to make best use of diversity techniques [98].

Further assistance may be offered by the channel environment, although this assistance is typically less readily

available at certain mmWave frequencies than at lower RF and microwave frequencies, due to increased signal attenuation at mmWave frequencies [20], [99]. However, in an atmospheric window such as that found at 28 GHz, the channel environment may provide propagation characteristics similar to those found at lower frequencies [1].

In addition to this, 5G wireless networks, operating at mmWave frequencies, may implement joint satellite and terrestrial connectivity through conventional CP mode techniques in order to provide the throughput promized by telecommunications providers [22].

Wave propagation using DP mode methods has been observed to increase capacity in a LoS channel where antenna alignment varies minimally with relative transmit-receive antenna spatial position, [61], [62], [100], and in more challenging longer range satellite environments that may augment terrestrial wireless services [22], [23], [64], [101]. Satellite communication design is useful for demonstrating the benefit of polarization diversity in three dimensions as it makes use of spherical geometry.

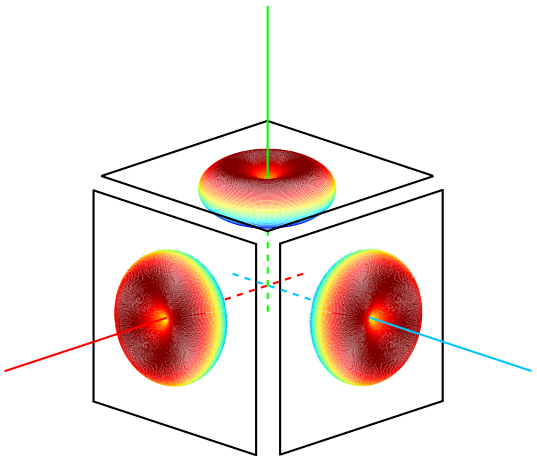

FIGURE 12. Tri-orthogonal arrangement of half-wavelength dipole modes. The familiar 'doughnut' radiation pattern of a half-wavelength dipole is associated with each of three orthogonal polarizations, or modes, represented by the red, green and blue coloured lines. Each polarization mode is orthogonal to an associated exploded cube face. In the case of half-wavelength dipole modes, each radiation pattern provides maximum gain in a direction in the plane of an associated cube face. Reduction of the cube to an infinitesimal volume enables the three orthogonal polarization mode radiation patterns to overlap. Together with high isolation between these modes, this overlap enables a desirable phase-centered system, minimising pattern asymmetry and providing the possibility of more than one polarization mode in any link direction.

The introduction of a third orthogonal dipole mode at the antenna, providing the potential of tri-orthogonal polarization diversity, potentially lessens the dependency on antenna alignment, and has been shown to increase capacity in a rich scattering environment [33], [34]. Figure 12 introduces radiation patterns associated with half-wavelength dipoles in a tri-orthogonal arrangement. Each of the three polarizations, or modes, represented by the red, green and blue coloured lines, is orthogonal to an exploded cube face. In the case of half-wavelength dipole modes, each radiation pattern

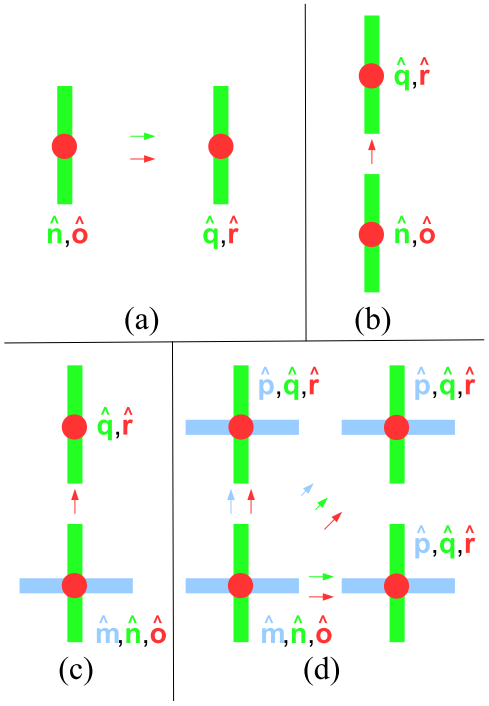

FIGURE 13. Mitigation of misalignment through a tri-orthogonal configuration of polarization modes. Mitigation of antenna misalignment is offered by the principle of tri-orthogonal polarization diversity: (a) full capacity is observed between the receiver configured using orthogonal polarization modes $\hat{\mathbf{q}}$, $\hat{\mathbf{r}}$, and the transmitter comprising orthogonal polarization modes $\hat{\mathbf{n}}$, $\hat{\mathbf{o}}$, due to perfect antenna alignment. Modes $\hat{\mathbf{o}}$ and $\hat{\mathbf{r}}$ are vertical polarized and so point upwards out of the paper; (b) at the receiver, half capacity is seen as only polarization mode $\hat{\mathbf{r}}$ is aligned with the transmitter; (c) the introduction of polarization mode $\hat{\mathbf{m}}$ at the transmitter provides no increase in capacity as only polarization mode $\hat{\mathbf{r}}$ is aligned to the transmitter; (d) the restoration of full capacity is achieved through inclusion of polarization mode $\hat{\mathbf{p}}$ at the receiver. In effect, at least two orthogonal polarization modes are offered in any link direction. Adapted from [107].

provides maximum gain in a direction in the plane of an associated cube face. For a desirable phase-centered system, in an attempt to reduce assymmetry of radiation pattern to a mimimum, the exploded cube is reduced to an infinitesimal volume. As such, the radiation patterns associated with each of the three orthogonal polarization modes overlap. Together with high isolation between these modes, this provides the possibility of more than one polarization mode in any given link direction.

As this article considers polarization diversity in three orthogonal directions, so the concept is demonstrated in Figure 13 through representation of orthogonal polarizations, or modes, solely. Nine subchannels are provided in Figure 13(d) by three orthogonal polarization modes, given as $\hat{\mathbf{m}}$, $\hat{\mathbf{n}}$, and $\hat{\mathbf{o}}$ at the transmitter and at the receiver, given as $\hat{\mathbf{p}}$, $\hat{\mathbf{q}}$, and $\hat{\mathbf{r}}$. Three signal transmissions, each polarized orthogonally to the other two, may be received by each of three orthogonally polarized receive branches at the receiver.

In a theoretical sense, orientation robustness of system capacity is provided as, due to symmetry of the tri-orthogonal

arrangement in six principal directions, DP mode signalling is provided in any link direction. In the case of a LoS channel, polarization diversity offers MIMO signalling. This may not always be possible for a system providing spatial diversity.

Performance may be enhanced by the benefit of a rich scattering environment [5], and this environment is typically cited in literature relating to MIMO systems [33], [34], [66]. At mmWave frequencies, such an environment may not be available. An arrangement of three orthogonal receive branch polarizations at the antenna may provide yet greater capacity if the orthogonality criteria between them is relaxed [102], [103], or if polarization diversity is used in tandem with spatial diversity [104]. However, these arrangements do not optimize capacity for all antenna orientations.

A combination of a LoS signal together with a non-line of sight (NLoS) component that arises from the channel environment forms a wireless channel that varies as a function of time. Scatterers in the channel may provide multipath signal components. For high SNR, the multipath effect may provide beneficial diversity at the receiver, enhancing signal reception. For low SNR, the multipath effect may render reception impossible, since scattering of the signal over the channel may weaken received components to the extent that they are unusable as components required to build up an intelligible signal at the receiver. Relative transmitter-receiver motion provides additional complexity to the analysis.

An orthogonal approach means that electric fields of propagating signals interact with the channel environment in an independent manner. As a result of this independence, system correlation is reduced. A combination of low correlation and changes in the channel environment provides a multitude of signal paths to the receiver. Data transfer rate may consequently be improved through no extra transmit power and negligible additional processing.

Terrestrial wireless networks typically employ vertically polarized antennas (e.g. AM and digital radio, cellular mobile networks) or horizontally polarized antennas (e.g. some television and FM radio broadcast networks). As a means to increase capacity, DP mode networks may employ two orthogonally polarized signals with no relative phase offset between them. This configuration is applied in [66], providing detail that highlights the effect of elevation angle at the receiver at conventional microwave frequencies.

Common antenna arrangements are vertical/horizontal mode and slant mode polarizations. Terrestrial signals are not subject to the ionospheric depolarization influence of Faraday rotation [105], [106]. As a consequence, terrestrial signals may typically be straighforwardly received by an antenna aligned with the transmitter configuration.

Signal propagation using a circularly polarized wave may be utilsed in problematic environments to provide signal reception. Circular polarization typically reduces transmitter range, as power is split equally over two orthogonal polarizations. This is undesirable at mmWave frequencies since linear transmit power is harder to maintain.

An additional issue is that a power transfer maximum is typically only seen in the instance of perfect alignment, or the center of a FoV, as seen from the perspective of the transmitter. For a mobile device, that typically does not enjoy perfect alignment with the transmitter, this has negative implications for link capacity. An additional degree of freedom at the receiver could mitigate this issue to an extent, in the form of an additional polarization branch orthogonal to those seen in conventional CP mode patch antenna receivers [22], [30].

Strong local scattering environments may require DCP mode wave propagation to circumvent channel effects, including depolarization. State-of-the-art satellite research introduces DCP mode wave propagation in the form of 2×2 MIMO systems using simultaneous LHCP mode and RHCP mode wave transmission [64]. As antenna alignment is essential to maintain link performance in a DCP mode system with evolving link geometry, tracking antennas are needed. Tracking systems are subject to physical breakdown, and are costly to maintain.

Reliance on a precise alignment of transmit and receive antennas in a LoS channel that typically provides little in the way of scattering is required for any of these systems if they are to provide full data transfer benefit. For a channel that provides a depolarizing mechanism, the receive antenna should provide a polarization state that is aligned with the electric field vector or electric field distribution of an impingent signal. Link effectiveness, including achievable capacity, is severely impacted by misalignment.

In Figure 6, losses due to polarization mismatch of aligned antennas are shown. The arrangements do not take into account misalignment of the antennas themselves, that may be encountered in a mobile environment and that further reduces link performance.

Link performance using tri-orthogonal antenna configurations is typically less sensitive to antenna misalignment and polarization mismatch, providing increased diversity gain and capacity in rich scattering channels [33], [34], [108], [109]. In effect, the configuration offers the promise of orientation robustness over all antenna orientations, provided that transmit signalling and receive processing allow for radio wave polarization as a function of link geometry at the receiver position. The additional degree of freedom offered by a third orthogonal polarization may provide link enhancement in a channel devoid of scattering effects, where misalignment may occur, as well as in a rich scattering channel environment where extreme depolarization may occur.

At the transmitter, in a plane perpendicular to the direction of propagation, the antenna configuration permits alignment with two orthogonal polarizations. In the direction of propagation, any signal component is negligible in the far-field. At the receive antenna, MIMO detection and interference cancellation are possible due to a tri-orthogonal polarisation diverse approach. This offers the potential of polarization-time coding [110], [111].

In this section, a three dimensional channel model is demonstrated that considers wireless link geometry between

a tri-orthogonal polarisation mode configuration applied at both transmitter and receiver. Simulations are performed through consideration of references at the FoV center [33], [112]. These references are respectively considered due to tri-orthogonal simulation and measurement of a receiver operating at low microwave frequencies and an analysis of capacity performance of linearly polarized antennas at higher mmWave frequencies. Both references provide findings in the form of a two dimensional line graph.

The model demonstrated in this paper introduces tri-orthogonality at both ends of a channel together with a three dimensional approach to analysis. Results suggest that a tri-orthogonal polarisation diverse approach enhances capacity performance in the absence of channel scatterers. This provides alignment robustness in typical mmWave region environments. The approach is useful as it delivers Rician fading simulations at mmWave frequencies through link decomposition into subchannels. This is a convenient technique for evaluating system performance. In addition, the approach offers the potential to introduce near-field and correlation effects while enabling signalling techniques that enhance link performance over the geometry of the FoV.

Calculation is performed of signal-to-noise (SNR) ratios that is used to demonstrate capacity over all antenna orientations. Comparison and contrast is provided of the tri-orthogonal configuration with both simulated mono- and bi-polarized systems and references.

Typically, DP mode link models implicitly assume ideal antenna alignment or use cross-polar correlations that are not dependent of link geometry [61]–[65]. Capacity enhancement through a tri-orthogonal configuration in channels both with and without channel scatterers is demonstrated through an approach considering three dimensional link geometry. While a three dimensional approach to modeling is observed at this point, prior research may not consider a tri-orthogonal configuration [66]–[68], nor provide a full assessment of link performance over all antenna orientations [69]. In addition, operation at frequencies where the effects of rich scattering environments may enhance performance is typically considered [70]–[72].

Attempting to combat link deterioration through increased link margin typically results in a system being overly sensitive to signal variation that may suffer the effects of amplifier saturation. A compromise exists, predominantly at higher frequencies, due to linear transmit power becoming more difficult to maintain. Systems are often more expensive as a consequence of failing to mitigate link deterioration. Minimisation of cost is of considerable value.

The effect of polarization mismatch is typically ignored in design at conventional operating frequencies. For a mobile system, ideal polarization alignment may only occur for a limited percentage of the time. Whereas this issue is mitigated by conventional systems, at higher mmWave frequencies a reduced availability of transmit power and a narrower beamwidth mean that polarization mismatch becomes a critical factor for link performance.

For certain antenna orientations, polarization mismatch may cause a -30 dB loss in power transfer, thus greatly reducing capacity. For RFID systems, that may be considered as a proxy for the Internet of Things [21], [113], the effect of polarization mismatch is considerable [114].

A. METHODS

The concept of link geometry is presented, together with its impact on link performance for a mmWave, tri-orthogonal system. MIMO signal propagation in a channel has been shown to improve link performance in rich scattering environments [5]. For channels devoid of a scattering mechanism, diversity gain is severely impacted. Polarization diverse MIMO signalling has demonstrated an improved performance in both terrestrial and satellite channel environments [31]–[33], [109], [115], [116].

Reduction of the impact of antenna orientation on link performance may be possible through a tri-orthogonal dipole configuration. In contrast to systems utilizing spatial diversity through three orthogonal polarization modes, and systems employing DP mode configurations, tri-orthogonal polarization diverse MIMO enables a phase centered smaller-scale tri-orthogonal antenna design to be achieved. Reconfigurable phase-centered radiation patterns offer the potential to enhance gain in a given link direction, appropriate for applications such as the IEEE (802.11ad) scheme at 60 GHz. As an example, the concept of massive MIMO looks to apply this technique in two dimensions, although it is largely confined to sub-5 GHz frequencies for the time being due to antenna array design complexity [117].

In the NLoS case, providing a rich scattering environment, a marked improvement in link performance has been shown using tri-orthogonal polarization diversity over that of DP mode diversity [33], [34]. Tri-orthogonal configurations provide a third degree of polarization freedom. An additional degree of freedom may provide benefit that may be extended over all antenna orientations. In the instance of deep fading with uni- or DP mode systems, a signal sent from a third orthogonal polarization mode is unlikely to experience the same fading.

Techniques currently used at RF and low microwave frequencies typically demonstrate a performance improvement through multipath effects in rich scattering environments. These techniques often do not take link geometry or physical effects in the channel into consideration [54]. A channel is time-dependent due to relative transmitter-receiver movement. Channel modeling requires the introduction of additional effects including Doppler phase shift and near-field effects [5].

An effective terrestrial channel model needs a deterministic LoS channel component as well as a stochastic NLoS channel component. The latter component dominates in the case of a stochastic fading channel. A normalized NLoS channel component may be modeled as a correlated complex Gaussian matrix consisting of elements with zero mean and unity standard deviation [118]. The approach

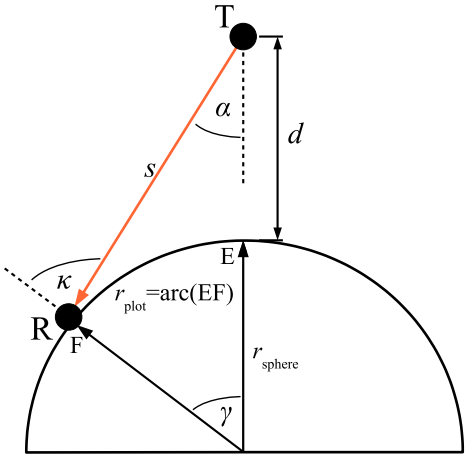

FIGURE 14. Link geometry of the terrestrial channel. The receiver R is located on a semi-circle. The proximal distance from T to R is *d*, while *s* is path length. Angles α, κ and γ define the relative position of R over the FoV. By rotation of this geometry about the FoV center by 360°, a spherical surface forming the ground range of the FoV is developed. Concentric paths on the sphere together with an incremental azimuthal step about the FoV center are user-defined. The model algorithm commences at the FoV center and works radially outward to the FoV perimeter where $\kappa = 90°$. After [107].

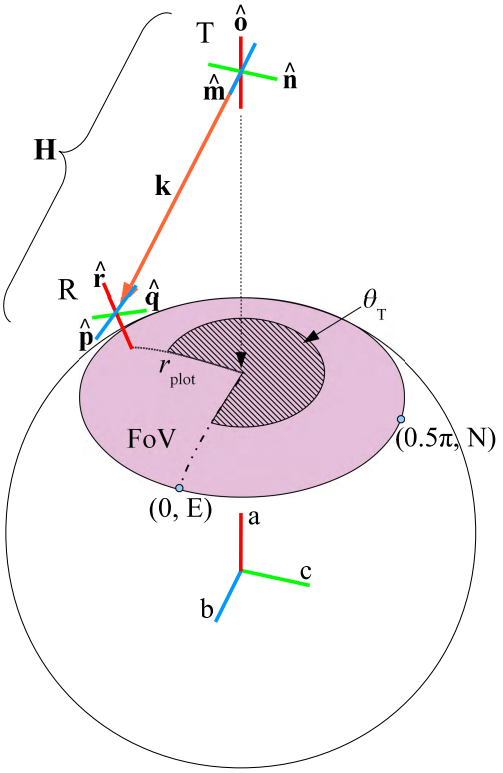

FIGURE 15. Tri-orthogonal configuration as a function of position in the terrestrial FoV. The unit polarisation branch $\hat{\mathbf{k}}$ is unique to a location in the FoV, and is a function of the azimuthal angle θ_T and the radial distance from the FoV center, r_{plot}. The movement of R in the FoV is decribed by easterly and northerly directions. In three dimensional space, half-wavelength configurations at R are given according to Equations (15), (16), and (17). The configurations at R, together with those at T, namely $\hat{\mathbf{m}}$, $\hat{\mathbf{n}}$ and $\hat{\mathbf{o}}$, then enable the determination of the variables needed for analysis of the channel, **H**, as a function of FoV position. Adapted from [107].

provides a determination of link performance over all antenna orientations.

Three mutually orthogonal unit vectors representing half-wavelength ($\lambda/2$) dipoles at both transmitter ($\hat{\mathbf{m}}$, $\hat{\mathbf{n}}$, $\hat{\mathbf{o}}$) and receiver ($\hat{\mathbf{p}}$, $\hat{\mathbf{q}}$, $\hat{\mathbf{r}}$) are assumed. These dipole modes provide orthogonally polarized radiation patterns at each antenna. Pattern distortion in the far-field, as a result of superposition, is avoided through a phase-centered approach that avoids any introduction of spatial diversity. No relative phase difference is assumed between transmitted signals. Figures 14 and 15 provide insight into the analysis method. The FoV and relevant nomenclature are now introduced.

A spherical surface is introduced, providing both a varying propagation distance and orientation to a receiver R. The point at which polarization branch $\hat{\mathbf{r}}$ is broadside to transmitter T defines the FoV perimeter. The model provides analysis of all antenna orientations.

In Figure 15, at T, polarization branch $\hat{\mathbf{m}}$ and the positive *b*-axis are in alignment, and this coincides with an azimuthal angle θ_T, as observed from T, of 0°. Polarization branch $\hat{\mathbf{n}}$ and the positive *c*-axis are aligned, coinciding with an azimuthal angle θ_T of 90°. Polarization branch $\hat{\mathbf{o}}$ and the positive *a*-axis are in alignment.

At the FoV center, at R, polarization branch $\hat{\mathbf{p}}$ and the positive *b*-axis are in alignment, and this coincides with an azimuthal angle θ_T of 0°. Polarization branch $\hat{\mathbf{q}}$ and the positive *c*-axis are aligned, coinciding with an azimuthal angle θ_T of 90°. Polarization branch $\hat{\mathbf{r}}$ and the positive *a*-axis are in alignment, when R is at the FoV center.

Movement of R within the FoV is given using easterly and northerly compass directions. These directions correspond to azimuthal angles of θ_T of 0° and 90° respectively. In Figure 15, polarization branch $\hat{\mathbf{p}}$ points in an easterly direction while polarization branch $\hat{\mathbf{q}}$ points in a northerly direction.

According to Figure 14 and the following equations, link geometry may be given.

$$\gamma = \frac{r_{\text{plot}}}{r_{\text{sphere}}} \tag{2}$$

$$s = \sqrt{u^2 + r_{\text{sphere}}^2 - 2ur_{\text{sphere}}\cos\gamma} \tag{3}$$

$$\kappa = \arcsin\left(\frac{u}{s}\sin\gamma\right) \tag{4}$$

$$\alpha = \arcsin\left(\frac{u}{s}\sin\gamma\right) - \gamma \tag{5}$$

$$\gamma_{\max} = \arccos\left(\frac{r_{\text{sphere}}}{u}\right) \tag{6}$$

$$s_{\max} = u\cos\alpha \tag{7}$$

$$\alpha_{\max} = \arcsin\left(\frac{r_{\text{sphere}}}{u}\right) \tag{8}$$

where u is $r_{\text{sphere}} + d$.

Viewing the FoV from T, rotation about the positive *a*-axis is considered positive in a counterclockwise sense, as

in Figure 15. At T, elevation is given by α. Elevation is given as 0° in the negative a-axis direction, else it is positive. At R, elevation is given by κ, with 0° in the positive a-axis direction, else it is positive. The tri-orthogonal configuration at R is at a distance s, from T. This distance varies as a function of FoV location. For an ideal system, received signal power over the FoV should be high and constant.

Power transfer over a subchannel is derived from the Friis formula [119]. For tri-orthogonal antenna configurations at both ends of a link, nine subchannel paths are generated. Each subchannel may be characterized by the Friis formula,

$$\frac{P_{\mathrm{R}}}{P_{\mathrm{T}}} = G_{\mathrm{T}}(\phi_{\mathrm{T}}, \theta_{\mathrm{T}}) G_{\mathrm{R}}(\phi_{\mathrm{R}}, \theta_{\mathrm{R}}) \left(\frac{\lambda}{4\pi s}\right)^2 e_{\mathrm{pol}} L_{\mathrm{atmos}}. \tag{9}$$

In Equation (9), the receiver is denoted by R, the transmitter by T, P is power, G is dipole gain, λ is transmitted wavelength, with T and R being separated by s. A polarization mismatch, e_{pol}, exists between two polarizations with L_{atmos} accounting for atmospheric attenuation at 60 GHz that is given here as 15 dBkm^{-1} [112].

A half-wavelength dipole provides a radiation pattern of gain G given by Equation (10) [30], [37], [120]. A 100 % dipole efficiency is assumed,

$$G(\theta, \phi) = \frac{1.64}{\sin^2 \theta} \cos^2 \left(\frac{\pi}{2} \cos \theta\right). \tag{10}$$

For polarization branch $\hat{\mathbf{o}}$ at T, angle θ is given by α, and this is seen in Figure 14. Minimum gain exists where α is 0°. Maximum gain exists where α is 90°, this not being in the FoV. The gain of polarization branch $\hat{\mathbf{o}}$ is not dependent of the azimuthal angle θ_{T}. For polarization branches $\hat{\mathbf{m}}$ and $\hat{\mathbf{n}}$ representing orthogonal polarization modes, angle θ can be determined by considering the inner product of a polarization branch and a unit vector $\hat{\mathbf{k}}$ representing propagation where,

$$\hat{\mathbf{k}} = \begin{bmatrix} -\cos\alpha \\ \cos\theta_{\mathrm{T}} \sin\alpha \\ \sin\theta_{\mathrm{T}} \sin\alpha \end{bmatrix}. \tag{11}$$

At R, for polarization branch $\hat{\mathbf{r}}$, angle θ is given by κ, this angle being sum of α and γ, as seen in Figure 14. For polarization branches $\hat{\mathbf{p}}$ and $\hat{\mathbf{q}}$, angle θ is given in the same manner as that for polarization branches $\hat{\mathbf{m}}$ and $\hat{\mathbf{n}}$, but with κ replacing α.

In Figure 16, profiles of gain are seen for the six half-wavelength dipoles associated with each of the six individual polarizations branches.

Polarization mismatch loss is incurred over a link when antenna configurations provide polarizations that are misaligned [30], [120]. In Figure 16, polarization mismatch e_{pol} may be determined for any half-wavelength dipole pair. For the half-wavelength dipole pair $\hat{\mathbf{r}}\hat{\mathbf{o}}$, the inner product in Equation (12) provides the polarization mismatch,

$$e_{\mathrm{pol}(\hat{\mathbf{r}}\hat{\mathbf{o}})} = |\hat{\mathbf{r}}_{\perp\mathbf{k}} \cdot \hat{\mathbf{o}}_{\perp\mathbf{k}}|^2 \tag{12}$$

where $\hat{\mathbf{r}}_{\perp\mathbf{k}}$ and $\hat{\mathbf{o}}_{\perp\mathbf{k}}$ are projections onto the plane perpendicular to the unit propagation vector $\hat{\mathbf{k}}$. As $\hat{\mathbf{r}}$ is a radial in nature,

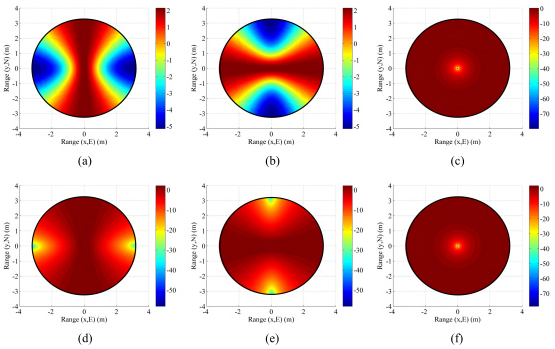

FIGURE 16. Gain (G) (dB) profiles of the six half-wavelength dipole modes over the terrestrial channel FoV. The polarized mode gains shown are: (a) $\hat{\mathbf{m}}$, (b) $\hat{\mathbf{n}}$, (c) $\hat{\mathbf{o}}$, (d) $\hat{\mathbf{p}}$, (e) $\hat{\mathbf{q}}$, (f) $\hat{\mathbf{r}}$. After [107].

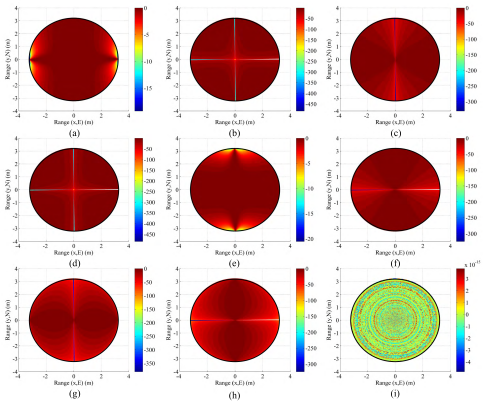

FIGURE 17. Polarization mismatch (e_{pol}) (dB) profiles for each unit dipole mode pair. The following polarized mode pair mismatches are shown: (a) $\hat{\mathbf{p}}\hat{\mathbf{m}}$, (b) $\hat{\mathbf{p}}\hat{\mathbf{n}}$, (c) $\hat{\mathbf{p}}\hat{\mathbf{o}}$, (d) $\hat{\mathbf{q}}\hat{\mathbf{m}}$, (e) $\hat{\mathbf{q}}\hat{\mathbf{n}}$, (f) $\hat{\mathbf{q}}\hat{\mathbf{o}}$, (g) $\hat{\mathbf{r}}\hat{\mathbf{m}}$, (h) $\hat{\mathbf{r}}\hat{\mathbf{n}}$, (i) $\hat{\mathbf{r}}\hat{\mathbf{o}}$. After [107].

and $\hat{\mathbf{o}}$ is a static dipole aligned in the zenith direction, so no polarization mismatch exists for this pair.

Any vector $\mathbf{v}$ may be projected onto the plane orthogonal to the propagation vector $\hat{\mathbf{k}}$,

$$\mathbf{v}_{\perp\mathbf{k}} = \left(\mathbf{I}_3 - \hat{\mathbf{k}}\hat{\mathbf{k}}^{\mathrm{T}}\right)\hat{\mathbf{v}}, \tag{13}$$

and normalization produces,

$$\hat{\mathbf{v}}_{\perp\mathbf{k}} = \frac{\mathbf{v}_{\perp\mathbf{k}}}{|\mathbf{v}_{\perp\mathbf{k}}|}. \tag{14}$$

In Figure 17, profiles are shown of polarization mismatch in all subchannels.

Orientation of the six half-wavelength dipoles represented by the six signal polarization unit vectors is described by the set of right-handed Cartesian axes in Figure 15. Axes a, The position of R on the sphere surface is described by axes a, b, c. Lengths $a1$, $b1$, $c1$ are along these axes repectively, and are normalized by r_{sphere}. Unit vectors representing orthogonal polarizations are respectively $\hat{\mathbf{m}} = [010]^{\mathrm{T}}$, $\hat{\mathbf{n}} = [001]^{\mathrm{T}}$, $\hat{\mathbf{o}} = [100]^{\mathrm{T}}$ and,

$$\hat{\mathbf{r}} = \begin{bmatrix} \cos\gamma \\ \cos\theta_{\mathrm{T}} \sin\gamma \\ \sin\theta_{\mathrm{T}} \sin\gamma \end{bmatrix} \tag{15}$$

where the superscript T denotes transpose.

Relative to the FoV center, the position on the spherical surface is required to calculate the orientation of $\hat{\mathbf{p}}$ and $\hat{\mathbf{q}}$,

$$\hat{\mathbf{p}} = \begin{bmatrix} -\sin(\text{atan}_2(b1,a1)) \\ \cos(\text{atan}_2(b1,a1)) \\ 0 \end{bmatrix} \tag{16}$$

$$\hat{\mathbf{q}} = \begin{bmatrix} -\sin(\arcsin(c1))\cos(\text{atan}_2(b1,a1)) \\ -\sin(\arcsin(c1))\sin(\text{atan}_2(b1,a1)) \\ \cos(\arcsin(c1)) \end{bmatrix} \tag{17}$$

where $\text{atan}_2(b1,a1)$ is described as,

$$\text{atan}_2(b1,a1) = \begin{cases} \arctan(\dfrac{b1}{a1}) & (a1 \succ 0) \\ \arctan(\dfrac{b1}{a1}) + \pi & (b1 \succeq 0, a1 \prec 0) \\ \arctan(\dfrac{b1}{a1}) - \pi & (b1 \prec 0, a1 \prec 0) \\ +\pi/2 & (b1 \succ 0, a1 = 0) \\ -\pi/2 & (b1 \prec 0, a1 = 0) \\ \text{undefined} & (b1 = 0, a1 = 0) \end{cases} \tag{18}$$

At the FoV center in Figure 15, $a1 = 1$, $b1 = 0$, and $c1 = 0$.

A matrix describing complex fading in a channel may be separated into the two components: a deterministic component ($\bar{\mathbf{H}}$), according to Equation (9) for each subchannel, and a stochastic component ($\tilde{\mathbf{H}}$) given by,

$$\mathbf{H} = \sqrt{\frac{K}{1+K}}\bar{\mathbf{H}} + \sqrt{\frac{1}{1+K}}\tilde{\mathbf{H}}. \tag{19}$$

In Equation (19), K is the Ricean K-factor [5]. A pure stochastic fading channel is produced by $K = 0$. A pure AWGN fading channel is produced by $K = \infty$. A complex Gaussian distribution is circularly symmetric, and refers to a random complex variable, $x + iy$, where the x and iy components are independent with zero mean and unit variance, $\aleph(0,1)$. A complex Gaussian component may be added over each subchannel through a complex Gaussian random matrix, $\tilde{\mathbf{H}}$.

Each element of this matrix is normalized by the square root of received power, $\sqrt{P_\text{R}}$, over each individual subchannel. This introduces a stochastic component to multipath fading, which may provide enhanced capacity performance over the channel through scattering and reflections, provided that signalling from T and reception at R take account of the radio wave polarization specific to the link geometry for the location of R during processing.

For this model, channel capacity is simulated at an instant in time for Ricean K-factors of 0 and ∞. Phase arguments of the deterministic LoS coefficients in $\bar{\mathbf{H}}$ are assumed to be zero. As a consequence, signal voltages propagating in the channel vary only by a magnitude change. All half-wavelength dipoles, and hence polarizations, at T are assumed to be colocated. The same assumption is made for half-wavelength dipoles, and hence polarizations, at R.

Equation (9) forms a basis for determining LoS power transfer over nine subchannels, that are unique to a FoV location.

The LoS power transfer is obtained from $\sqrt{P_\text{R}/P_\text{T}}$ [121], this being a function of signal voltage amplitude changes as the signal propagates in the channel.

A factor denoting polarization mismatch, e_pol, includes projections via Equation (13). The 3×3 matrix $\mathbf{H}$ is at most rank two in the case of no channel scatterers. Multipath, or scattering effects, increase channel rank, and therefore capacity, as the channel approaches a case of Rayleigh fading. In effect, a typical channel may provide localized uncorrelated fading through reflections of the propagating signal within zones close to the transmitter and the receiver.

As a result, channel rank is not degraded to the same extent as propagation in between these zones where propagation distance is far larger than the radius of such a zone [58]. The addition of a third orthogonal radiating dipole provides both antenna and polarization diversity over the channel. As a consequence, channel rank is not impacted in the same way as for conventional CP mode techniques.

The probability of multipath in the case of a scattering channel is increased by the use of omnidirectional antennas, that in turn provides the possibility of increasing capacity over the FoV.

For a polarization diverse antenna design, in a terrestrial Rayleigh fading environment, correlation is near negligible [32], [58]. In [122] and [123], designs providing a measured maximum mutual port coupling between polarizations of -35 dB are demonstrated.

A channel matrix $\mathbf{H}$ for each receive antenna location, and subsequent orientation, in the FoV may be given according to the calculation of the nine subchannels using Equation (9). In the case of M receiver elements and N transmitter elements, a channel matrix is given as,

$$\mathbf{H} = \begin{bmatrix} h_{\hat{\mathbf{p}}\hat{\mathbf{m}}} & h_{\hat{\mathbf{p}}\hat{\mathbf{n}}} & h_{\hat{\mathbf{p}}\hat{\mathbf{o}}} \\ h_{\hat{\mathbf{q}}\hat{\mathbf{m}}} & h_{\hat{\mathbf{q}}\hat{\mathbf{n}}} & h_{\hat{\mathbf{q}}\hat{\mathbf{o}}} \\ h_{\hat{\mathbf{r}}\hat{\mathbf{m}}} & h_{\hat{\mathbf{r}}\hat{\mathbf{n}}} & h_{\hat{\mathbf{r}}\hat{\mathbf{o}}} \end{bmatrix} \tag{20}$$

where the matrix coefficients in Equation (20) represent signal transfer between a unit dipole receive-transmit pair.

For M receivers and N transmitters, capacity is given by Equation (21) [58], [110], [111], [124] as,

$$C = \log_2 \left| \left(\mathbf{I}_M + \frac{P_\text{T}}{P_\text{N} N} \mathbf{H}\mathbf{H}^\dagger \right) \right| \tag{21}$$

where P_T is the total transmit power at T, P_N is the noise power at R, $\mathbf{I}$ represents an identity matrix, and † denotes the Hermitian transpose.

With unit transmit power assumed in all cases, a 3×3 tri-orthogonal system is observed to effectively spread transmit power over the FoV. Additional diversity is provided at R over conventional CP mode and DP mode receive antenna designs. The tri-orthogonal arrangement provides orientation robustness, rather than concentrating power at the FoV center, where typically the system operates optimally.

B. RESULTS

To provide a basis for simulation, comparison at the FoV center with prior work in the field is introduced [33], [112]. Data taken at the FoV center is shown in Figure 18 for operation at 2.55 GHz in a channel with Rayleigh fading characteristics [125]. The positive a-axis is used to align antennas at T and at R as per Figure 15.

As expected, the Shannon capacity limit is approached for both the 1 × 1 system and that of [112], due to perfect alignment. An identical analysis applies to the case of DP mode propagation. A difference in capacity exists between that of the simulated tri-orthogonal NLoS case and the case of prior work [33]. This results from only the receiver being a tri-orthogonal configuration in the latter, where the transmitter is a three fold, linearly polarized system.

As a consequence of a tri-orthogonal configuration only at R, the system demonstrates a three fold increase in capacity over that of a uni-polarized system. This is not the case for a tri-orthogonal arrangement at T and at R due to link geometry. This difference in tri-orthogonal system capacity is clearly observed in Figure 18.

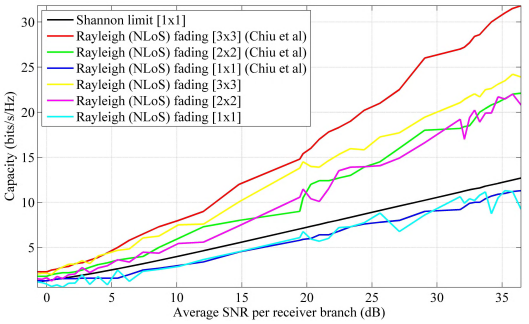

FIGURE 18. Simulated capacity performance at 2.55 GHz of uni-polarized, dual-polarized, and tri-orthogonal configurations. Capacity performance is provided as a function of average SNR per receiver branch at the FoV center in a Rayleigh (NLoS) fading channel, according to prior work [33]. A Rician factor K of 10^{-2} is used. The antenna configuration at T is ideally aligned with that at R along the positive a-axis, as in Figure 15. The discrepancy in capacity between the tri-orthogonal, or 3 × 3, configuration of the presented model and the simulated and measured 3 × 3 configuration in the work of [33], results from a non-orthogonal configuration being adopted at T in the latter. After [107].

In Figure 19 a uni-polarized LoS capacity comparison is shown, for operation at 60 GHz, of the channel model with that of prior work in this area [112]. Extension to both DP mode and tri-orthogonal systems is made, as all considered configurations base subchannel element coefficients on an average SNR at a location in the FoV, acquired through link analysis. A proximal distance, d, ranging from 1–20 m provides for the determination of average SNR values.

Results are provided for three dimensional link geometry over a FoV. An operating frequency of 60 GHz is employed, together with a transmit power of 40 dBm, a bandwidth of 7 GHz, and a system noise temperature [112] of 290 K. A close proximity wireless personal area network (WPAN) is considered as, at the FoV center, a propagation distance

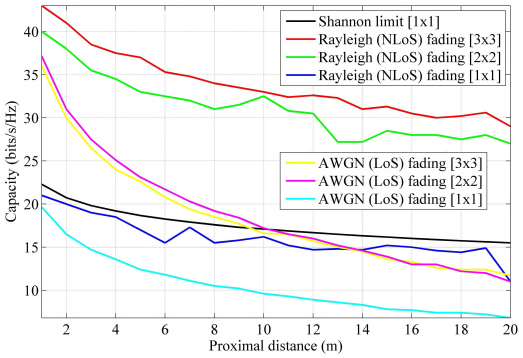

FIGURE 19. Relative capacity performance at the FoV center of uni-polarized, dual-polarized, and tri-orthogonal configurations at 60 GHz. Capacity performance is provided as a function of distance from the FoV center, or d, as shown in Figure 14 in both deterministic AWGN and stochastic Rayleigh fading channels. Applied Ricean factors of 10^{3} and 10^{-2} are respectively used. The antenna configuration at T is ideally aligned with that at R along the positive a-axis, as in Figure 15. After [107].

of 1 m is employed. A spherical radius of 6 m is employed, together with a channel exponent of 1.55 [112].

Ricean K-factors of $K = 0$ and $K = \infty$ are used. These values provide channel extremes, ranging from a pure Rayleigh [112], [126] to a pure AWGN fading channel.

From figures 21 to 24, we observe the following points:

- in both the AWGN and Rayleigh fading regimes, the 3 × 3 system shows a superior performance to that of the dual-polarized and uni-polarized systems over a major part of the FoV.
  Over the FoV, capacity is more consistent. The Shannon capacity limit is approached in the instance of a Rayleigh fading channel.
- at the FoV center, the tri-orthogonal system is subject to a decrease in performance in comparison to the dual-polarized system. This is as a result of redundancy of the third orthogonal unit dipole pair, or $\hat{\mathbf{r}}\hat{\boldsymbol{\theta}}$, at the FoV center. The decrease in capacity is most prominent in the AWGN channel, but is a reasonable trade-off for increased orientation robustness over the major part of the FoV.
  In Figure 19, it is noteworthy that the capacity disadvantage is not observed for the tri-orthogonal system. This is due to an average of capacity being obtained at positions that are infinitesimally close to the exact FoV center.
- in the AWGN fading channel, capacity for the 3 × 3 system is observed to be highest at four offset positions that are approximately 10° off-center, and at 45°, 135°, 215° and 305° azimuth. At these points, a three fold increase in capacity is observed compared to the 1 × 1 system. Capacity is seen to approach the 3 × 3 Shannon capacity limit. Orientation robustness is provided even in the absence of a channel scatterers.
- in a channel where Rayleigh fadiong dominates, a capacity increase is noted that results from the addition of a third orthogonal polarization branch over the major part of the FoV. An approximate three fold increase in

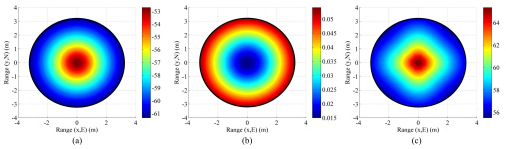

FIGURE 20. Channel environment parameters as a function of FoV position. Profiles shown are: (a) free space path loss (dB), (b) atmospheric loss L_{atmos} (dB), and (c) average SNR per receiver branch for a tri-orthogonal system (dB). After [107].

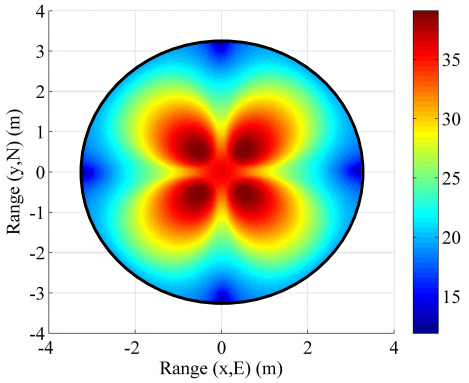

FIGURE 21. Tri-orthogonal capacity performance (bits/s/Hz) in a deterministic AWGN fading channel. Simulated results are given in a FoV format for all receive antenna orientations and, by extension, all system orientations. The system operates with a transmit power of 40 dBm, an operating frequency of 60 GHz, a bandwidth of 7 GHz, while a system noise temperature of 290 K is employed. At the FoV center, the propagation distance is 1 m. This distance corresponds to a close proximity wireless personal area network (WPAN). Displacement of R over the spherical surface is achieved by using a spherical radius of 6 m. Results suggest a maximum capacity that is offset in four positions from the FoV center. At the FoV center, polarization modes $\hat{\mathbf{r}}$ and $\hat{\mathbf{o}}$ are redundant, and this redundancy is mitigated at the four offset positions while providing near optimal alignment of dipole pairs, or polarization modes, $\hat{\mathbf{p}}$ and $\hat{\mathbf{m}}$, and $\hat{\mathbf{q}}$ and $\hat{\mathbf{n}}$. After [107].

capacity, compared to the uni-polarized case, is seen at all locations around the FoV center. Capacity is seen to approach a tri-orthogonal Shannon capacity limit. This increased capacity zone is more marked than for the AWGN channel. This is due to an increased possibility of propagation between two perfectly misaligned polarization branches in a rich scattering environment.

- at the FoV center, an advantage in channel capacity is observed in a stochastic Rayleigh fading environment comapred to a AWGN fading environment. This advantage increases as a function of increasing proximal distance, or decreasing average SNR per receiver branch, before remaining constant. A channel with an abundance of channel scatterers is seen to be more assistive for lower values of SNR.

C. PRACTICAL DESIGN

Of course, the benefit of tri-orthogonal polarization diversity cannot be implemented unless an appropriate design can be demonstrated. Previous designs [33], [34] have increased the third dimension of any design, and so have made it more voluminous with obvious implications where size is a constraint.

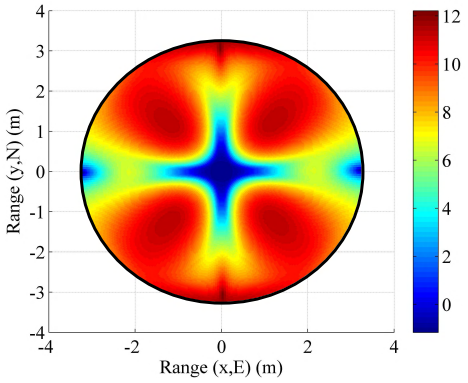

FIGURE 22. Superiority of capacity performance (bits/s/Hz) in a deterministic AWGN fading channel of a tri-orthogonal system over that of a dual-polarized system. Simulated results are given in a FoV format for all receive antenna orientations and, by extension, all system orientations. The system operates with a transmit power of 40 dBm, an operating frequency of 60 GHz, a bandwidth of 7 GHz, while a system noise temperature of 290 K is employed. At the FoV center, the propagation distance is 1 m. This distance corresponds to a close proximity wireless personal area network (WPAN). Displacement of R over the spherical surface is achieved by using a spherical radius of 6 m. At the FoV center, redundancy of polarization modes $\hat{\mathbf{r}}$ and $\hat{\mathbf{o}}$ provides a slight dip in capacity performance of the tri-orthogonal system when compared with the dual-polarized system. The tri-orthogonal arrangement is observed to provide enhanced capacity over the majority of the FoV, when compared with the dual-polarized system. After [107].

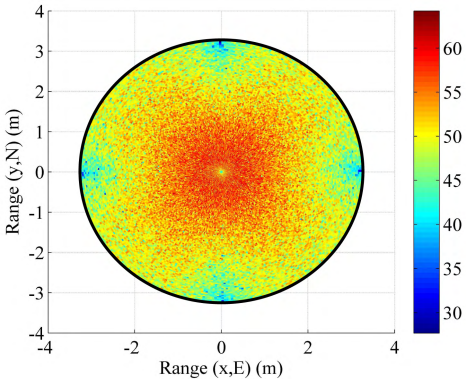

FIGURE 23. Tri-orthogonal capacity performance (bits/s/Hz) in a stochastic Rayleigh fading channel. Simulated results are given in a FoV format for all receive antenna orientations and, by extension, all system orientations. The system operates with a transmit power of 40 dBm, an operating frequency of 60 GHz, a bandwidth of 7 GHz, while a system noise temperature of 290 K is employed. At the FoV center, the propagation distance is 1 m. This distance corresponds to a close proximity wireless personal area network (WPAN). Displacement of R over the spherical surface is achieved by using a spherical radius of 6 m. Polarization modes $\hat{\mathbf{r}}$ and $\hat{\mathbf{o}}$ are redundant at the FoV center, although this redundancy is mitigated by the nature of the Rayleigh fading channel. After [107].

In this context, a planar design that fulfills the criteria of tri-orthogonal polarization diversity is given in [122], and this is shown in Figure 28.

The design offers the possibility of beam steering in three dimensions, with the potential of dual polarization over all link directions in an extended field-of-view (FoV), such as may be required in a mobile terrestrial context [107], [127]. As coverage of next generation wireless communications

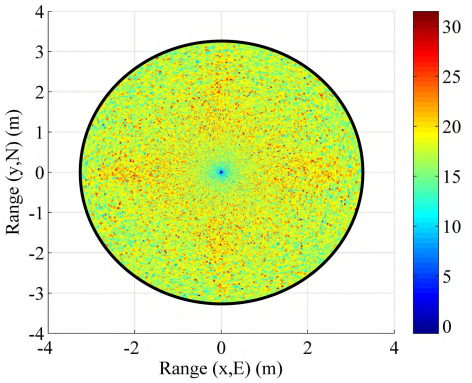

FIGURE 24. Superiority of capacity performance (bits/s/Hz) in a stochastic Rayleigh fading channel of a tri-orthogonal system over that of a dual-polarized system. Simulated results are given in a FoV format for all receive antenna orientations and, by extension, all system orientations. The system operates with a transmit power of 40 dBm, an operating frequency of 60 GHz, a bandwidth of 7 GHz, while a system noise temperature of 290 K is employed. At the FoV center, the propagation distance is 1 m. This distance corresponds to a close proximity wireless personal area network (WPAN). Displacement of R over the spherical surface is achieved by using a spherical radius of 6 m. At the FoV center, redundancy of polarization modes $\hat{\mathbf{r}}$ and $\hat{\mathbf{o}}$ provides a slight decrease in capacity performance of the tri-orthogonal system when compared with the dual-polarized system. The area of inferior performance is smaller than that observed in the AWGN channel, due to the nature of the Rayleigh fading channel. The tri-orthogonal arrangement is observed to provide enhanced capacity over the majority of the FoV, when compared with the dual-polarized system. After [107].

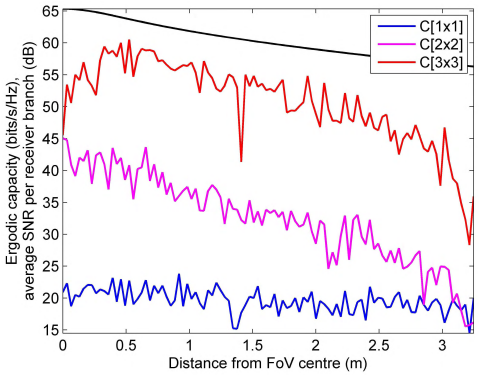

FIGURE 25. Profile of stochastic Rayleigh fading channel capacity (bits/s/Hz) at an azimuthal angle of $\theta_{\mathbf{T}} = 0°$ for uni-polarized, dual-polarized and tri-orthogonal systems. This diagram represents system capacity observed as the arrangement of orthogonal half-wavelength dipoles at the receiver are displaced on the sphere of radius 6 m from the FoV center, or alignment with the positive *a*-axis, in the positive *c*-axis direction in Figure 15 to the FoV edge. The 1 × 1, or uni-polarized system considers propagation between the dipole pair, or polarization modes, $\hat{\mathbf{p}}$ and $\hat{\mathbf{m}}$. The 2 × 2, or dual-polarized system, considers propagation using dipoles, or polarization modes, $\hat{\mathbf{p}}$, $\hat{\mathbf{q}}$ at R and $\hat{\mathbf{m}}$, $\hat{\mathbf{n}}$ at T. The 3 × 3, or tri-orthogonal system considers propagation using dipoles, or polarization modes, $\hat{\mathbf{p}}$, $\hat{\mathbf{q}}$, and $\hat{\mathbf{r}}$ at R and $\hat{\mathbf{m}}$, $\hat{\mathbf{n}}$, and $\hat{\mathbf{o}}$ at T. The average SNR per receiver branch as a function of distance from the FoV center is also shown. After [107].

looks to extend to a satellite communicating to a ground receiver, so the benefits of tri-orthogonal polarization diversity can be applied in a non-geosynchronous satellite channel at the receiver [60].

In addition, a sequential feeding network may be applied to the planar tri-orthogonal antenna design that adds

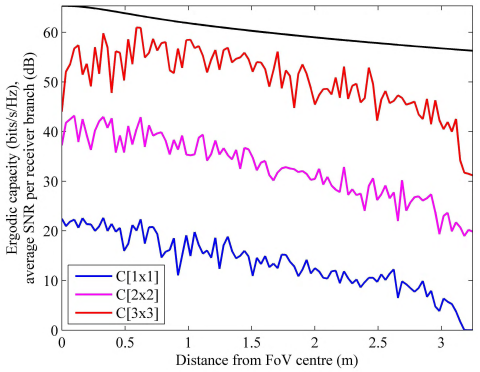

FIGURE 26. Profile of stochastic Rayleigh fading channel capacity (bits/s/Hz) at an azimuthal angle of $\theta_{\mathbf{T}} = 90°$ for uni-polarized, dual-polarized and tri-orthogonal systems. This diagram represents system capacity observed as the arrangement of orthogonal half-wavelength dipoles at the receiver is displaced on the sphere of radius 6 m from the FoV center, or alignment with the positive *a*-axis, in the positive *c*-axis direction in Figure 15 to the FoV edge. The 1 × 1, or uni-polarized system, considers propagation between the dipole pair, or polarization modes, $\hat{\mathbf{p}}$ and $\hat{\mathbf{m}}$. The 2 × 2, or dual-polarized system, considers propagation using dipoles, or polarization modes, $\hat{\mathbf{p}}$, $\hat{\mathbf{q}}$ at R and $\hat{\mathbf{m}}$, $\hat{\mathbf{n}}$ at T. The 3 × 3, or tri-orthogonal system, considers propagation using dipoles, or polarization modes, $\hat{\mathbf{p}}$, $\hat{\mathbf{q}}$, and $\hat{\mathbf{r}}$ at R and $\hat{\mathbf{m}}$, $\hat{\mathbf{n}}$, and $\hat{\mathbf{o}}$ at T. The average SNR per receiver branch as a function of distance from the FoV center is also shown. After [107].

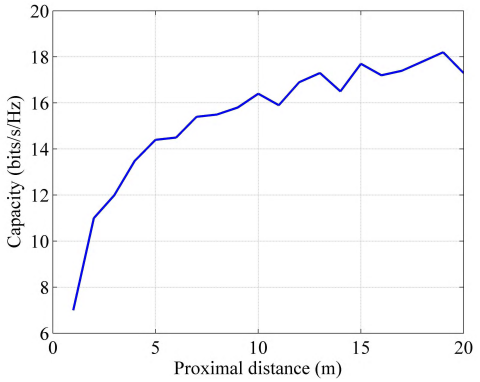

FIGURE 27. Capacity advantage (bits/s/Hz) of a stochastic Rayleigh fading channel over that of a deterministic AWGN fading channel. The tri-orthogonal antenna arrangement at R is in perfect alignment with the tri-orthogonal antenna arrangement at T. As such, polarization mode $\hat{\mathbf{p}}$ is aligned with the positive *b*-axis, polarization mode $\hat{\mathbf{q}}$ is aligned with the positive *c*-axis, and polarization mode $\hat{\mathbf{r}}$ is aligned with the positive *a*-axis in Figure 15. The capacity observed in a rich scattering Rayleigh fading channel compared to the capacity observed in a AWGN channel, devoid of scatterers, is shown for propagation at the FoV center, or along the neagative *a*-axis, as a function of proximal distance. The proximal distance is shown in Figure 14 as *d*. After [107].

a polarization orthogonal to the antenna surface to a circularly polarized system. As such, a third orthogonal polarization above that of a conventional planar antenna design is offered. The antenna provides a high level of symmetry and orthogonality, and three dimensional beam steering is demonstrable [123]. Such a possibility provides the ability to steer a radiation pattern, and so gain, of an antenna in a particular direction, and so mitigate to a certain degree, the limitation of transmit power at mmWave frequencies. The design may be extended into massive MIMO systems, as it

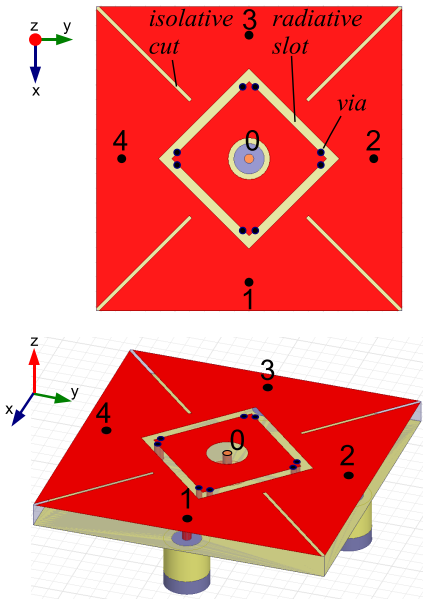

FIGURE 28. Antenna operation is through differential, or antiphase, feeding of opposing port pairs 1 and 3, or 2 and 4. Field cancellation results at the center, providing high isolation between either of two resulting orthogonal broadside modes and a vertically polarized monopole mode fed at the center of the design through port 0. Tri-orthogonal polarization diversity is possible and port excitation combinations may beam steer radiated energy in three dimensions through a common radiative square slot. After [122].

remains planar in nature, providing beam steering techniques in three dimensions through three orthogonal polarizations.

IV. CONCLUSION

Mobile data traffic is growing rapidly. A next generation of wireless communications, or 5G, is proposed to increase data transfer rates and coverage through operation in the mmWave range of the electromagnetic spectrum.

In the literature, a rich scattering channel advantage is typically included in references that consider the benefits of MIMO operation at conventional RF and low microwave frequencies. Furthermore, analysis is often limited to perfect alignment, or a few specific orientations. Until now, conventional polarization technqiues have sufficed, as antenna misalignment and polarisation mismatch issues have been mitigated by an abundance of transmit power and spatial diversity.

Limitations exist with regard to continuing these policies in a mmWave channel context. Efficient exploitation of radiated energy is required to meet the 5G proposals of increased data rate and coverage. Operation of terrestrial wireless systems at mmWave frequencies may not be assisted by multipath effects, as a consequence of lower transmit power capability, higher spreading loss, and a reduced number of channel scatterers compared to those within a conventional microwave terrestrial channel. The importance of polarization cannot be over-emphasized in this regard.

In this paper, a presented model suggests that the inclusion of a third polarization at both transmitter and receiver, orthogonal to the antenna radiating surface, provides orientation robustness and overall increased capacity performance for communication in a short-range mmWave channel over a majority of a FoV that considers all antenna orientations in channel extremes.

A design that is phase-centred avoids pattern distortion in the far-field. Through introduction of phased feeding techniques to such a design, beam steering of antenna radiation patterns becomes possible. Tri-orthogonal polarization diversity offers the potential to beam steer radiated energy towards an antenna over a wide range of angles, through relative phasing techniques that may be enhanced by changes in relative wave magnitude.

Remaining within conventional planar size constraints has proved an issue for prior tri-orthogonal antenna design. To this end, a novel antenna providing tri-orthogonal polarization diversity in a planar form is highlighted. The design suggests that conventional size constraints need not restrict polarization diversity methods for the next generation of wireless communications.

APPENDIX A
Maxwell's EQUATIONS

A. IN VACUO

For a region of space devoid of charges and currents, the equations of Maxwell are given as a set of coupled, first order, partial differential equations for the electrical vector $\mathbf{E}$ and magnetic vector $\mathbf{B}$. These equations form the foundation of classical electromagnetics and are given in the following form,

$$\nabla \cdot \mathbf{E} = 0 \quad \text{(Faraday's Law)} \tag{22}$$

$$\nabla \cdot \mathbf{B} = 0 \quad \text{(Ampère's Law)} \tag{23}$$

$$\nabla \times \mathbf{E} = -\frac{\partial \mathbf{B}}{\partial t} \quad \text{(Gauss' Law)} \tag{24}$$

$$\nabla \times \mathbf{B} = \mu_0 \epsilon_0 \frac{\partial \mathbf{E}}{\partial t} \quad \text{(Coulomb's Law).} \tag{25}$$

Applying a curl operation to Equations (24) and (25) yields the following expressions respectively,

$$\begin{aligned} \nabla \times (\nabla \times \mathbf{E}) &= \nabla(\nabla \cdot \mathbf{E}) - \nabla^2 \mathbf{E} \\ &= -\nabla \times \frac{\partial \mathbf{B}}{\partial t} = -\frac{\partial}{\partial t}(\nabla \times \mathbf{B}) \\ &= -\mu_0 \epsilon_0 \frac{\partial^2 \mathbf{E}}{\partial t^2} \end{aligned} \tag{26}$$

$$\begin{aligned} \nabla \times (\nabla \times \mathbf{B}) &= \nabla(\nabla \cdot \mathbf{B}) - \nabla^2 \mathbf{B} = \nabla \times \left(\mu_0 \epsilon_0 \frac{\partial \mathbf{E}}{\partial t} \right) \\ &= \mu_0 \epsilon_0 \frac{\partial}{\partial t}(\nabla \times \mathbf{E}) = -\mu_0 \epsilon_0 \frac{\partial^2 \mathbf{B}}{\partial t^2} \end{aligned} \tag{27}$$

where the permittivity of free space, ϵ_0 and permeability of free space μ_0, are constants that are respectively found in Coulomb's law and the Biot-Savart law. Since $\nabla \cdot \mathbf{E} = 0$ and $\nabla \cdot \mathbf{B} = 0$, so these expressions reduce to,

$$\nabla^2 \mathbf{E} = \mu_0 \epsilon_0 \frac{\partial^2 \mathbf{E}}{\partial t^2} \tag{28}$$

and

$$\nabla^2 \mathbf{B} = \mu_0 \epsilon_0 \frac{\partial^2 \mathbf{B}}{\partial t^2}. \tag{29}$$

This process generates separate equations for **E** and **B**, which are of second order. In a vacuum, each Cartesian component of **E** and **B** satisfies a three-dimensional wave equation, or,

$$\nabla^2 f = \mu_0 \epsilon_0 \frac{\partial^2 f}{\partial t^2}. \tag{30}$$

The solution of this equation is a wave. Maxwell's equations suggest that a vacuum supports the propagation of an electromagnetic wave, travelling with a velocity of light, c, or $3 \times 10^8 \text{ms}^{-1}$.

B. MONOCHROMATIC PLANE WAVES

For a light wave, which is an electromagnetic wave, different frequencies in the visible range correspond to different colours. Different frequencies correspond to different wavelengths of electromagnetic waves, and these waves may collectively be referred to as monochromatic waves. Electromagnetic waves, travelling in a direction that we shall refer to as z, with no x and y dependence, are known as plane waves. Plane waves are made of fields that are uniform over every plane orthogonal to the direction of propagation, z. The coexisting electric and magnetic fields of such plane waves assume the following form,

$$\mathbf{E}(z, t) = \mathbf{E}_0 \exp^{\text{i(kz-}\omega\text{t)}} \tag{31}$$

$$\mathbf{B}(z, t) = \mathbf{B}_0 \exp^{\text{i(kz-}\omega\text{t)}}. \tag{32}$$

The vectors $\mathbf{E}_0$ and $\mathbf{B}_0$ are the electrical and magnetic complex amplitudes of the propagating electromagnetic wave. Through substitution of Equations (31) and (32) into Equations (28) and (29), we are led to,

$$c = \frac{\omega}{k} \tag{33}$$

where c is the velocity of light and ω is the angular frequency of the electromagnetic wave. The wavenumber k is related to the wavelength of the wave by Equation (34),

$$\lambda = \frac{2\pi}{k}. \tag{34}$$

Classically, the direction of **E** is used to specify the polarization of the electromagnetic wave. In empty space, the wave equations for **E** and **B** are derived from Maxwell's equations. Indeed, the wave equation must be obeyed by every solution to Maxwell's equations in empty space. Since $\nabla \cdot \mathbf{E} = 0$ and $\nabla \cdot \mathbf{B} = 0$, it follows that $E_{0z} = B_{0z} = 0$.

In other words, electromagnetic waves are transverse in nature. The electric and magnetic fields are orthogonal to the direction of propagation, as shown in Figure 29. Equation (22), or Faraday's law, implies a relation between the dielectric and magnetic amplitudes. In compact form, this relationship may be given as,

$$\mathbf{B}_0 = \frac{k}{\omega}(\hat{\mathbf{z}} \times \mathbf{E}_0) = \frac{1}{c}(\hat{\mathbf{z}} \times \mathbf{E}_0). \tag{35}$$

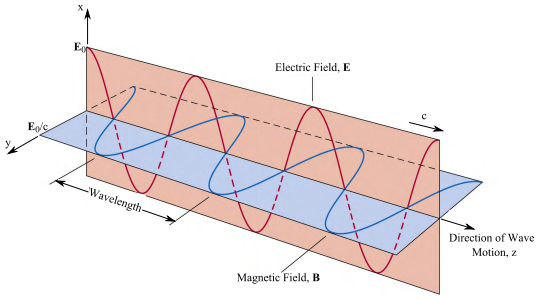

FIGURE 29. An electromagnetic wave consists of a sinusoidal electric field distribution and associated sinusoidal magnetic field distribution. The fields are orthogonal to each other and in phase with other, and are both orthogonal to the direction of propagation. Adapted from [128].

The electric and magnetic vectors, **E** and **B**, are in phase and are orthogonal. We may introduce a wave vector, **k**, pointing in the direction of propagation z, with a magnitude equal to the wave number k. The scalar product $\mathbf{k}\cdot\mathbf{r}$, where **r** is a radial vector, is the appropriate generalisation of kz where,

$$\mathbf{E}(\mathbf{r}, t) = E_0 \mathbf{e} \exp^{\text{i}(\mathbf{k}\cdot\mathbf{r}-\omega t)} \tag{36}$$

$$\mathbf{B}(\mathbf{r}, t) = \frac{1}{c} E_0 (\mathbf{n} \times \mathbf{e}) \exp^{\text{i}(\mathbf{k}\cdot\mathbf{r}-\omega\text{t})} = \frac{1}{c}(\mathbf{n} \times \mathbf{E}) \tag{37}$$

The vector **n** is a unit vector in the direction of propagation, where $\mathbf{n} = \frac{\mathbf{k}}{k}$. The polarization vector is given as **e**. As **E** is transverse, so $\mathbf{n} \cdot \mathbf{e} = 0$.

C. LINEAR, CIRCULAR AND ELLIPTICAL POLARIZATION

The plane wave with components given in Equations (36) and (37) is a wave with its electric field vector in the direction **e**. A wave of this nature is said to be linearly polarized and possess a polarization vector $\mathbf{e}_1 = \mathbf{e}$.

We introduce a second linearly polarized wave with a polarization vector $\mathbf{e}_2 \neq \mathbf{e}_1$. This wave is linearly independent of the first. As a consequence, we may write the two waves as,

$$\mathbf{E}_1(\mathbf{r}, t) = E_1 \mathbf{e}_1 \exp^{\text{i}(\mathbf{k}\cdot\mathbf{r}-\omega\text{t})} \tag{38}$$

and

$$\mathbf{E}_2(\mathbf{r}, t) = E_2 \mathbf{e}_2 \exp^{\text{i}(\mathbf{k}\cdot\mathbf{r}-\omega t)}. \tag{39}$$

Coexisting magnetic waves may be given in the form,

$$\mathbf{B}_{1,2} = \frac{1}{c}(\mathbf{n} \times \mathbf{E}_{1,2}) \tag{40}$$

The two waves may be combined to provide a plane wave in general form propagating in the direction of $\mathbf{k} = k\mathbf{n}$,

$$\mathbf{E}(\mathbf{r}, t) = \mathbf{E}_1(\mathbf{r}, t) + \mathbf{E}_2(\mathbf{r}, t) = (E_1 \mathbf{e}_1 + E_2 \mathbf{e}_2) \exp^{\text{i}(\mathbf{k}\cdot\mathbf{r}-\omega t)}. \tag{41}$$

The amplitudes E_1 and E_2 are complex numbers, allowing a potential relative phase difference to exist between waveforms of non-identical linear polarization. Alternatively, a phase difference may be represented by an additional term

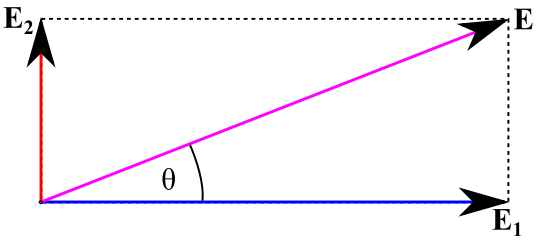

FIGURE 30. The direction of polarization of an electromagnetic wave is described according to the electric field vector. Two linearly polarized electric fields, described respectively by electric field vectors $\mathbf{E_1}$ and $\mathbf{E_2}$, that are in phase with each other and are travelling in the same direction of propagation, combine to form a resultant linearly polarized electric field distribution shown here by the electric field vector **E**, or the magenta line. The resultant electric field vector may be described according to the angle theta between the resultant electric field vector **E** and the electric vector $\mathbf{E_1}$.

in the complex exponent of one of the propagating waves. Three possibilities of plane wave exist:

- If E_1 and E_2 have the same phase then Equation (41) represents a wavefront demonstrating **linear polarization**, as shown in Figure 30. The polarization vector of the resultant waveform is given by $\tan\theta = \mathrm{E_2/E_1}$ with respect to $\mathbf{e}_1$, with a magnitude of $\sqrt{E_2^2 + E_1{}^2}$.
- If a 90° phase exists between E_1 and E_2, which are of the same magnitude, then Equation (41) represents a wavefront exhibiting **circular polarization** of the form,

$$\mathbf{E}(\mathbf{r}, t) = \mathbf{E}_1(\mathbf{r}, t) + \mathbf{E}_2(\mathbf{r}, t) = E_0(\mathbf{e}_1 \pm i\mathbf{e}_2)\exp^{\mathrm{i}(\mathbf{k}\cdot\mathbf{r}-\omega t)} \tag{42}$$

with E_0 the common real amplitude. Axes are chosen such that a wave is propagating in a positive z direction, with $\mathbf{e}_1$ and $\mathbf{e}_2$ being repsectively in the x and y directions. Actual electric field components are found from the real part of Equation (42),

$$E_{\mathrm{x}}(\mathbf{r}, t) = \mathbf{E}_0 \cos(kz - \omega t) \tag{43}$$

and

$$E_{\mathrm{y}}(\mathbf{r}, t) = \mp\mathbf{E}_0 \sin(kz - \omega t). \tag{44}$$

At a given fixed point in space, the fields of Equations (43) and (44) provide a resultant electric vector with constant magnitude, sweeping around in a circle at an angular frequency ω, as shown in Figure 31.

For the upper sign of Equation (42), the rotation is counterclockwise when the observer is facing into the oncoming wave. The wave is deemed to be right hand circularly polarized in antenna design. Conversely, for the lower sign in Equation (42), the rotation is clockwise, and so the wave is deemed to be left hand circularly polarized.

- Two counter-rotating circularly polarized waves may form an equally acceptable basis for describing a general state of polarization, known as **elliptical polarization**, of which several cases may be observed in Figure 32.

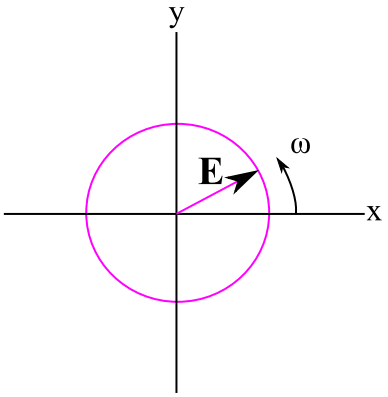

FIGURE 31. Circular polarization. Providing a relative phase difference of 90° between two orthogonal linearly polarized electric field distributions of the same magnitude, and travelling in the same direction of propagation, results in a circularly polarized electric field vector. The resultant wave polarization, shown here by the magenta line, is observed to rotate with angular frequency ω about a fixed point as it propagates through a medium. The sense of rotation is dictated by the advancement or retardation of one of the linearly polarized electric field distributions with respect to the other.

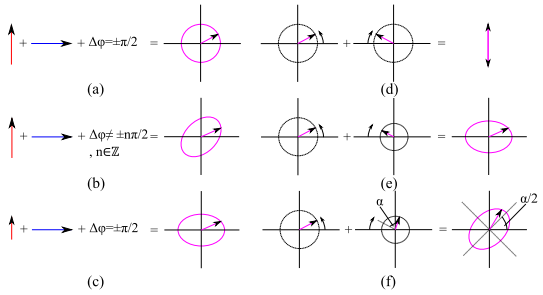

FIGURE 32. Linear and circular polarizations are the extreme forms of the more general case of elliptical polarization. The cases of elliptical polarization are most simply understood when two orthogonal linearly polarized waves travelling in the same direction of propagation towards the observer combine with: (a) identical magnitudes and a phase difference of 90° to produce circular polarization, (b) identical magnitudes and a phase difference that is non-zero and that is not a multiple of 90° to produce elliptical polarization with 45° rotated semi-major and semi-minor axes, (c) a 90° phase difference but non-identical magnitudes to produce elliptical polarization. Cases of elliptical polarization may also be demonstrated by two counter rotating circularly polarized electric field vectors with: (d) identical phase and identical magnitudes to produce linear polarization, (e) identical phases and non-identical magnitudes to produce elliptical polarization, (f) the introduction of non-identical phases to (e) causing the axes of the ellipse to be rotated by an angle ($\alpha/2$), where the angle α represents the relative phase difference between the counter rotating electric field vectors.

Vertical linear polarization is described by counter-rotating circularly polarized waves experiencing no relative phase shift between them, as shown in Figure 32 (d). As a relative phase shift is introduced between the counter-rotating electric vector tips, so linear polarization veers away from the vertical, becoming horizontal with a 180 ° relative phase shift. This is shown in Figure 34.

Using two counter-rotating circularly polarized waves, we may represent Equation (41) for a general state of polarization through the introduction of complex

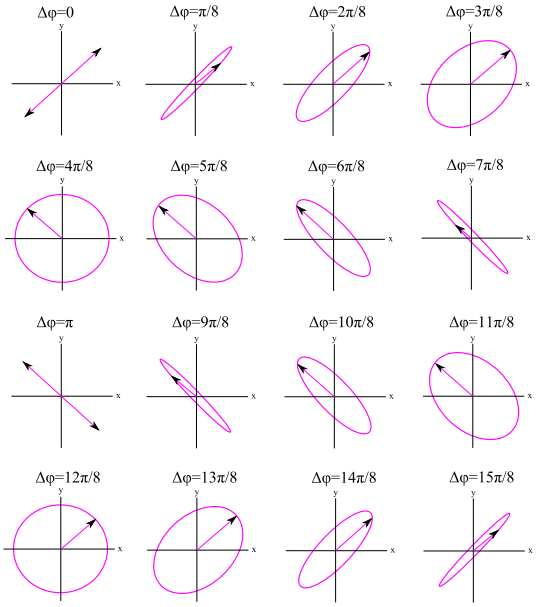

FIGURE 33. The effect of relative phase on two orthogonal polarization modes. By combining a vertically polarized electric field distribution with a horizontally polarized electric field distribution, of identical magnitude and both travelling in the same direction of propagation towards the observer, it is possible to cycle through resultant wave linear, elliptical and circular polarizations by altering the relative phase difference between the two waves. In this diagram, increments of $\pi/8$ radians are sequentially added to this relative phase difference, providing the cycling of resultant wave polarizations indicated. The ellipse axes are rotated by 45°, due to the identical magnitude of the vertically polarized and horizontally polarized electric field distributions.

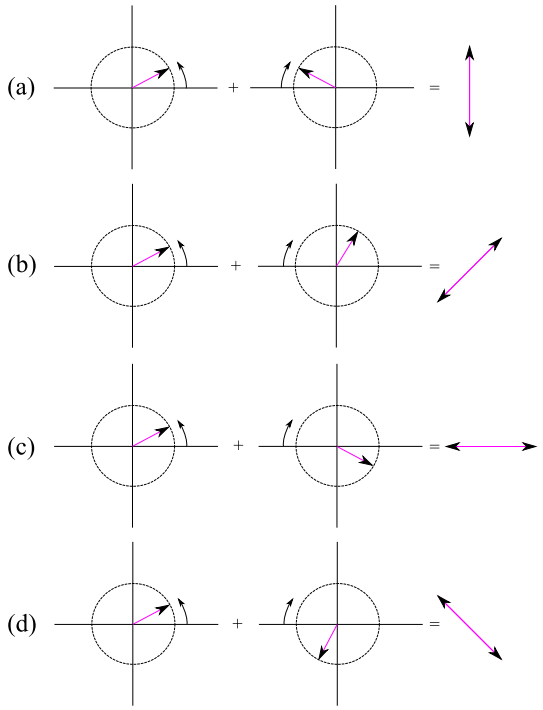

FIGURE 34. Resultant polarization through circular polarization combination. Two counter-rotating circularly polarized electric field vectors of the same magnitude travelling in the same direction of propagation towards the observer may combine to form each of the four specific cases shown. The cases are: (a) relative phase difference of 0° results in a vertically polarized electric field distribution, (b) relative phase difference of 90° results in a slant polarized electric field distribution, (c) relative phase difference of 180° results in a horizontally polarized electric field distribution, (d) relative phase difference of 270° results in a slant polarized electric field distribution that is 90° rotated about the direction of propagation in relation to (b).

orthogonal unit vectors,

$$\mathbf{e}_{\pm} = \frac{1}{\sqrt{2}}(\mathbf{e}_1 \pm i\mathbf{e}_2) \tag{45}$$

to give,

$$\mathbf{E}(\mathbf{r}, t) = (E_+\mathbf{e}_+ + E_-\mathbf{e}_-)\exp^{\mathrm{i}(\mathbf{k}\cdot\mathbf{r}-\omega t)}. \tag{46}$$

In Equation (46), E_+ and E_- are complex amplitudes. For E_+ and E_- with non-identical magnitudes but identical phase, Equation (46) signifies an elliptically polarized wave. The principal axes of the ellipse are in the $\mathbf{e}_1$ and $\mathbf{e}_2$ directions, this being shown in Figure 32 (e). The ratio of principal axes is $|(1 + r)/(1 - r)|$, where $r = E_-/E_+$.

With a relative phase difference between the amplitudes, $E_-/E_+ = re^{\mathrm{i}\alpha}$, and the ellipse traced out by the vector has its axes rotated by an angle $(\alpha/2)$, as shown in Figure 32 (f). A linearly polarized wave is obtained when $r = \pm 1$.

By cycling the phase of two orthogonal linear polarized waves of identical magnitude, we may produce the elliptical polarizations observed in Figure 33.

In Figure 35, various forms of linear, circular and elliptical polarization are shown using combinations of linearly polarized waves travelling towards the observer. From observation of Figures 32, 33, 34, and 35, the interconnection of linear, circular, and elliptical polarization is evident.

D. ELECTROMAGNETIC WAVES IN MATTER

In regions of matter devoid of free charges and free currents, Maxwell's equations become,

$$\nabla \cdot \mathbf{D} = 0 \quad \text{(Faraday's Law)} \tag{47}$$

$$\nabla \cdot \mathbf{B} = 0 \quad \text{(Ampère's Law)} \tag{48}$$

$$\nabla \times \mathbf{E} = -\frac{\partial \mathbf{B}}{\partial t} \quad \text{(Gauss' Law)} \tag{49}$$

$$\nabla \times \mathbf{H} = \frac{\partial \mathbf{D}}{\partial t} \quad \text{(Coulomb's Law)}\,. \tag{50}$$

For linear matter, $\mathbf{D} = \epsilon\mathbf{E}$ and $\mathbf{H} = \frac{1}{\mu}\mathbf{B}$. If the matter is also homogenous, then Maxwell's equations reduce to,

$$\nabla \cdot \mathbf{E} = 0 \quad \text{(Faraday's Law)} \tag{51}$$

$$\nabla \cdot \mathbf{B} = 0 \quad \text{(Ampère's Law)} \tag{52}$$

$$\nabla \times \mathbf{E} = -\frac{\partial \mathbf{B}}{\partial t} \quad \text{(Gauss' Law)} \tag{53}$$

$$\nabla \times \mathbf{B} = \mu\epsilon\frac{\partial \mathbf{E}}{\partial t} \quad \text{(Coulomb's Law)}. \tag{54}$$

In effect, the difference between electromagnetic waves propagating in a linear homogenous medium and those

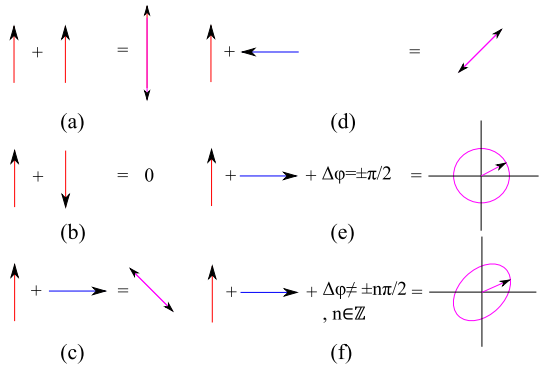

FIGURE 35. Resultant polarization through linear polarization combination. Presented are general forms of polarization resulting from the combination of two linearly polarized electric field distributions of identical magnitude travelling in the same direction of propagation towards the observer. Images shown are: (a) two vertically polarized in-phase electric vectors combine to form a vertically polarized electric field vector, (b) two vertically polarized electric vectors in anti-phase combine to form no electric field distribution, (c) vertically polarized and horizontally polarized electric field vectors that are in phase combine to form a slant polarized electric field vector, (d) vertically polarized and horizontally polarized electric field vectors that are in anti-phase combine to form a slant polarized electric field vector that is 90° rotated about the direction of propagation in relation to (c), (e) vertically polarized and horizontally polarized electric field vectors with a relative phase difference of 90° between them combine to form a circularly polarized electric field vector, (f) vertically polarized and horizontally polarized electric field vectors with a relative phase difference between them that is non-zero and that is not a multiple of 90° combine to form an elliptically polarized electric field vector with 45° rotated semi-major and semi-minor axes.

propagating in a vacuum is the inclusion of relative permittivity and permeability into Coulomb's law in the former case. Through a linear homogenous medium, electromagnetic waves travel with a velocity,

$$v = \frac{1}{\sqrt{\mu\epsilon}} = \frac{c}{n} \tag{55}$$

where

$$n = \sqrt{\frac{\mu\epsilon}{\mu_0\epsilon_0}} \tag{56}$$

is the index of refraction. In the case of most non-ferromagnetic materials, μ is very close to μ_0. As a result of this, we may say that $n \approx \sqrt{\epsilon_r}$, where ϵ_r is the dielectric constant of the medium.

APPENDIX B
TRANSMITTING AND RECEIVING ANTENNAS

A. EFFECTIVE AREA OF AN ANTENNA

In the model employed in this article, we consider linear antennas. The effective area of a linear antenna is not equal to the physical antenna area. This is in contrast to dish or horn antennas, where the effective area is typically 55–65% of the physical area for the former and 60–80% for the latter. Antennas typically fall into two classes: (i) fixed-gain configurations such as linear antennas where gain G is frequency independent and (ii) fixed-area configurations where gain G increases quadratically with frequency f. In this paper, our model considers a half-wave dipole antenna, which is a linear antenna with a maximum gain given as 1.64, this being in a direction of propagation orthogonal to the dipole.

B. ANTENNA NOISE TEMPERATURE

The received signal from a non-geosynchronous satellite is extremely weak due to the large free space path loss that it experiences during propagation. This loss is typically of the order of 150 dB or more, resulting in a received signal being of the order of picowatts. Detection of a faint signal requires the receiver system to sustain a noise level lower than the received signal. Several sources may introduce noise into the receiving system. As well as the desired signal, the receiving antenna may pick up noisy signals from the several sources including the sky, the weather, the ground, as well as other natural or man-made noise sources. Noise signals, impingent on the receiver from various directions, may be weighted according to the antenna gain. From this weighting, a weighted average noise power for the receiver at the output terminals of the antenna may be calculated. As an example, for an antenna pointing in the zenith direction, noise will be picked up through its sidelobes due to thermal noise and reflected signals from the ground. Ohmic losses in the antenna provide an additional noise source. Any antenna output that propagates in a lossy feed line, such as a transmission line or waveguide, before arriving at the receiver circuits is attenuated by the feed line. In addition, the feed line will introduce additional thermal noise.

From the feed line, the output is then passed into a LNA, pre-amplifying the signal and introducing only a limited quantity of thermal noise. Indeed, a critical property of the receiving system is the low-noise nature of the LNA. From the LNA, the output signal is then passed to system downconverters, IF amplifiers, and bandpass filters. These subsystems all introduce their own gain and thermal noise factors. Collectively, the system provides a cascade of receiver components. Receiver system performance can only be guaranteed by ensuring that the sum total of all the noises injected by these constituent parts remains at an acceptably low level, in comparison to the amplified wanted signal. For a receiver system operating with a bandwidth of B Hz, the average power P_N (in Watts) of a noise source is given by means of an equivalent temperature T. The average power is defined as,

$$P_N = kTB \tag{57}$$

where k is the Boltzmanns constant $= 1.3803 \times 10_{-23}$ W/Hz·K and T is in degrees Kelvin [37]. A convenient way to express the noise power is through the temperature T. This temperature does not have to equal the physical temperature of the source. However, this temperature T is indeed the physical temperature for a thermal source.

APPENDIX C
EFFECTIVE LENGTH AND POLARIZATION MISMATCH

For an antenna, the polarization properties of an electric field $\mathbf{E}$ depend on the transverse component of a radiation

vector $\mathbf{F}_\perp$ where,

$$\mathbf{E} = -jk\eta\frac{e^{-jkr}}{4\pi r}\mathbf{F}_\perp = -jk\eta\frac{e^{-jkr}}{4\pi r}(F_\theta\hat{\mathbf{\Theta}} + F_\phi\hat{\mathbf{\Phi}}). \quad (58)$$

An effective length vector $\mathbf{h}$ of an antenna may be defined in terms of the radiation vector $\mathbf{F}_\perp$, and the input current I_{in} to the terminals of an antenna,

$$\mathbf{h} = -\frac{\mathbf{F}_\perp}{I_{\text{in}}}. \quad (59)$$

In general, $\mathbf{h}$ is a function of (θ, ϕ). The electric field $\mathbf{E}$ may then be written as,

$$\mathbf{E} = -jk\eta\frac{e^{-jkr}}{4\pi r}I_{\text{in}}\mathbf{h}. \quad (60)$$

Motivation for the definition of $\mathbf{h}$ is provided by the case of a vertical Hertzian dipole antenna, which is shown to have $\mathbf{h} = I\sin\theta\hat{\mathbf{\Theta}}$. As a consequence of the reciprocity principle, the open circuit voltage V at the terminals of a receiving antenna may be given in terms of the incident electric field $\mathbf{E}_{\text{i}}$ and the effective length $\mathbf{h}$ by,

$$V = \mathbf{E}_{\text{i}} \cdot \mathbf{h}. \quad (61)$$

The normal definition of the effective area A of an antenna and the resulting power gain $G = 4\pi A/\lambda^2$, where λ is the operating wavelength, depend on idealised assumptions. These assumptions are that a conjugate-match exists between the receive antenna and its load, as well as the antenna polarization matching that of the incident wave.

Characterization of the degree of polarization mismatch that may exist between the incident field and the antenna is assisted by the effective length, ultimately leading to a modified area-gain relationship.

Polarization and load mismatch factors may be defined by,

$$e_{\text{pol}} = \frac{|\mathbf{E}_{\text{i}} \cdot \mathbf{h}|^2}{|\mathbf{E}_{\text{i}}|^2|\mathbf{h}|^2}. \quad (62)$$

$$e_{\text{load}} = \frac{4R_{\text{L}}R_{\text{A}}}{|Z_{\text{L}} + Z_{\text{A}}|^2} = 1 - |\Gamma_{\text{load}}|^2 \quad (63)$$

where

$$\Gamma_{\text{load}} = \frac{Z_{\text{L}} - Z_{\text{A}}^*}{Z_{\text{L}} + Z_{\text{A}}}. \quad (64)$$

We include the load mismatch factor for completeness. In the article, the load mismatch factor is set to unity.

The effective area may then be written as,

$$A(\theta, \phi) = \frac{\eta|\mathbf{h}|^2}{4R_{\text{A}}}e_{\text{load}}e_{\text{pol}}. \quad (65)$$

Finally, we may give the modified gain-area relationship as Equation (66),

$$A(\theta, \phi) = e_{\text{load}}e_{\text{pol}}\frac{\lambda^2}{4\pi}G(\theta, \phi) \quad (66)$$

where G is the power gain of the antenna under scrutiny, and λ is the operating wavelength.

We may assume that the incident field originates at some antenna with its own effective length $\mathbf{h}_{\text{i}}$. By making this assumption, $\mathbf{E}_i$ will be proportional to $\mathbf{h}_i$, and hence the polarization mismatch factor may be written as,

$$e_{\text{pol}} = \frac{|\mathbf{h}_{\text{i}} \cdot \mathbf{h}|^2}{|\mathbf{h}_{\text{i}}|^2|\mathbf{h}|^2} = |\hat{\mathbf{h}}_{\text{i}} \cdot \hat{\mathbf{h}}|^2 \quad (67)$$

where

$$\hat{\mathbf{h}}_{\text{i}} = \frac{\mathbf{h}_{\text{i}}}{|\mathbf{h}_{\text{i}}|} \quad (68)$$

and

$$\hat{\mathbf{h}} = \frac{\mathbf{h}}{|\mathbf{h}|}. \quad (69)$$

For a load that is conjugate-matched, we have $e_{\text{load}} = 1$. For an incident field that has matching polarization with the antenna, or $\mathbf{h}_{\text{i}} = \mathbf{h}^*$, then $e_{\text{pol}} = 1$. In this article, we assume the load to be conjugate-matched. We examine the mitigation of polarization mismatch through tri-orthogonal polarization diversity.

REFERENCES

[1] T. S. Rappaport *et al.*, "Millimeter wave mobile communications for 5G cellular: It will work!" *IEEE Access*, vol. 1, pp. 335–349, 2013.

[2] J. Nanzer, *Microwave and Millimeter-Wave Remote Sensing for Security Applications* (Artech House Remote Sensing Library). Norwood, MA, USA: Artech House, 2012. [Online]. Available: https://books.google.co.uk/books?id=v9sF0aV_llcC

[3] M. Tonouchi, "Cutting-edge terahertz technology," *Nature Photon.*, vol. 1, no. 2, pp. 97–105, 2007.

[4] P. Adhikari. (2008). Understanding millimeter wave wireless communication. Loea Corporation. [Online]. Available: http://www.loeacom.com/pdf%20files/L1104-WP_Understanding%20MMWCom.pdf

[5] A. Goldsmith, *Wireless Communications*. Cambridge, U.K.: Cambridge Univ. Press, 2005.

[6] I. E. Telatar and D. N. C. Tse, "Capacity and mutual information of wideband multipath fading channels," *IEEE Trans. Inf. Theory*, vol. 46, no. 4, pp. 1384–1400, Jul. 2000.

[7] R. L. Van Tuyl, "Unlicensed millimeter wave communications. A new opportunity for MMIC technology at 60 GHz," in *IEEE 18th Annu. Gallium Arsenide Integr. Circuit (GaAs IC) Symp. Tech. Dig.*, Nov. 1996, pp. 3–5, doi: 10.1109/GAAS.1996.567624.

[8] A. M. Niknejad and H. Hashemi, Eds., *mm-Wave Silicon Technology: 60 GHz and Beyond* (Integrated Circuits and Systems). New York, NY, USA: Springer, 2008. [Online]. Available: https://books.google.co.uk/books?id=poDOIsRlfQwC

[9] D. H. Werner and Z. H. Jiang, Eds., *Electromagnetics of Body Area Networks: Antennas, Propagation, and RF Systems*. Hoboken, NJ, USA: Wiley, 2016. [Online]. Available: https://books.google.co.uk/books?id=ey2pDAAAQBAJ

[10] Quotient Associates Ltd. *5G Candidate Band Study: Study on the Suitability of Potential Candidate Frequency Bands Above 6 GHz for Future 5G Mobile Broadband Systems*, accessed on 2015. [Online]. Available: http://stakeholders.ofcom.org.uk/binaries/consultations/above-6ghz/qa-report.pdf

[11] T. S. Rappaport. *The Coming Renaissance of the Wireless Communications Age*, accessed on 2014. [Online]. Available http://wireless.engineering.nyu.edu/presentations/NYSWAX.pdf

[12] Above Ground Level Media Group. *FCC Looks Ever Higher for Spectrum to Meet 5G Wireless Demand*, accessed on 2015. [Online]. Available: http://www.aglmediagroup.com/fcc-looks-ever-higher-for-spectrum-to-meet-5g-wireless-demand/

[13] Qualcomm Technologies Inc. *FCC Vote Will Pave the Path for 5G Advancements to Mobilize mmWave [UPDATED]*, accessed on 2016. [Online]. Available: https://www.qualcomm.com/news/onq/2016/07/12/upcoming-fcc-vote-will-pave-path-5g-advancements-mobilize-mmwave

[14] Cellular Telephone Industries Association. *Wireless Telecommunications Bureau Seeks Comment on the State of Mobile Wireless Competition*, accessed on 2016. [Online]. Available: http://www.ctia.org/docs/default-source/fcc-filings/160531-filed-ctia-mobile-wireless-competition-report-comments.pdf

[15] Federal Communications Commission. *Fact Sheet: Spectrum Frontiers Proposal to Identify, Open Up Vast Amounts of New High-Band Spectrum for Next Generation (5G) Wireless Broadband*, accessed on 2016. [Online]. Available: https://apps.fcc.gov/edocs_public/attachmatch/DOC-339990A1.pdf

[16] Federal Communications Commission. *Amendment of the Commission's Rules With Regard to Commercial Operations in the 3550–3650 MHz Band*, accessed on 2015. [Online]. Available https://apps.fcc.gov/edocs_public/attachmatch/FCC-12-148A1_Rcd.pdf

[17] S. Sun, T. S. Rappaport, R. W. Heath, Jr., A. Nix, and S. Rangan, "MIMO for millimeter-wave wireless communications: Beamforming, spatial multiplexing, or both?" *IEEE Commun. Mag.*, vol. 52, no. 12, pp. 110–121, Dec. 2014.

[18] G. R. MacCartney, Jr., and T. S. Rappaport, "73 GHz millimeter wave propagation measurements for outdoor urban mobile and backhaul communications in New York City," in *Proc. IEEE Int. Conf. Commun. (ICC)*, Jun. 2014, pp. 4862–4867, doi: 10.1109/ICC.2014.6884090.

[19] A. Alkhateeb, J. Mo, N. Gonzalez-Prelcic, and R. W. Heath, Jr., "MIMO precoding and combining solutions for millimeter-wave systems," *IEEE Commun. Mag.*, vol. 52, no. 12, pp. 122–131, Dec. 2014.

[20] P. Smulders, "Exploiting the 60 GHz band for local wireless multimedia access: Prospects and future directions," *IEEE Commun. Mag.*, vol. 40, no. 1, pp. 140–147, Jan. 2002.

[21] K. Ashton, "That 'Internet of Things' thing," *RFiD J.*, vol. 22, no. 7, pp. 97–114, 2009.

[22] K. M. Mak, H. W. Lai, K. M. Luk, and C. H. Chan, "Circularly polarized patch antenna for future 5G mobile phones," *IEEE Access*, vol. 2, pp. 1521–1529, 2014, doi: 10.1109/ACCESS.2014.2382111.

[23] B. Evans, O. Onireti, T. Spathopoulos, and M. A. Imran, "The role of satellites in 5G," in *Proc. IEEE 23rd Eur. Signal Process. Conf. (EUSIPCO)*, Aug./Sep. 2015, pp. 2756–2760, doi: 10.1109/EUSIPCO.2015.7362886.

[24] J. Gubbi, R. Buyya, S. Marusic, and M. Palaniswami, "Internet of Things (IoT): A vision, architectural elements, and future directions," *Future Generat. Comput. Syst.*, vol. 29, no. 7, pp. 1645–1660, 2013.

[25] Libellium Comunicaciones Distribuidas. *Smart World*, accessed on 2014. [Online]. [Online]. Available: http://www.libelium.com/libelium-smart-world-infographic-smart-cities-internet-of-things/

[26] Ericsson. *Ericsson Research Blog: 5G Challenges and Research*, accessed on 2015. [Online]. Available: https://www.ericsson.com/research-blog/5g/5g-challenges-research/

[27] Institute of Electrical and Electronics Engineers. *IEEE Conference on Standards for Communications and Networking*, accessed on 2016. [Online]. Available: http://cscn2016.ieee-cscn.org/CFP/CSCN16-CFP.pdf

[28] European Union. *The 5G Infrastructure Public Private Partnership*, accessed on 2016. [Online]. Available: https://5g-ppp.eu/5g-ppp-phase-1-projects/

[29] B. Y. Toh, R. Cahill, and V. F. Fusco, "Understanding and measuring circular polarization," *IEEE Trans. Edu.*, vol. 46, no. 3, pp. 313–318, Aug. 2003.

[30] C. A. Balanis, *Antenna Theory: Analysis and Design*. Hoboken, NJ, USA: Wiley, 2005.

[31] W. Lee and Y. Yeh, "Polarization diversity system for mobile radio," *IEEE Trans. Commun.*, vol. 20, no. 5, pp. 912–923, Oct. 1972.

[32] A. M. D. Turkmani, A. A. Arowojolu, P. A. Jefford, and C. J. Kellett, "An experimental evaluation of the performance of two-branch space and polarization diversity schemes at 1800 MHz," *IEEE Trans. Veh. Technol.*, vol. 44, no. 2, pp. 318–326, May 1995.

[33] C. Y. Chiu, J. B. Yan, and R. D. Murch, "Compact three-port orthogonally polarized MIMO antennas," *IEEE Antennas Wireless Propag. Lett.*, vol. 6, pp. 619–622, Dec. 2007.

[34] M. R. Andrews, P. P. Mitra, and R. de Carvalho, "Tripling the capacity of wireless communications using electromagnetic polarization," *Nature*, vol. 409, pp. 316–318, Jan. 2001, doi: 10.1038/35053015.

[35] Samsung Electronics Inc. *Samsung Electronics Sets 5G Speed Record at 7.5 Gbps, Over 30 Times Faster Than 4G LTE*, accessed on 2014. [Online]. Available: http://www.samsung.com/uk/news/local/samsung-electronics-sets-5g-speed-record-at-7-5gbps-over-30-times-faster-than-4g-lte

[36] University of Surrey. *University-of-Surrey-Achieves-5G-Speeds-of-1Tbps*, accessed on 2015. [Online]. Available: http://www.v3.co.uk/v3-uk/news/2396249/exclusive-university-of-surrey-achieves-5g-speeds-of-1tbps

[37] D. M. Pozar, *Microwave Engineering*, 4th ed. Hoboken, NJ, USA: Wiley, 2011.

[38] H. J. Liebe, T. Manabe, and G. A. Hufford, "Millimeter-wave attenuation and delay rates due to fog/cloud conditions," *IEEE Trans. Antennas Propag.*, vol. 37, no. 12, pp. 1612–1617, Dec. 1989.

[39] Z. Pi and F. Khan, "An introduction to millimeter-wave mobile broadband systems," *IEEE Commun. Mag.*, vol. 49, no. 6, pp. 101–107, Jun. 2011.

[40] H. Hashemi and S. Raman, Eds., *mm-Wave Silicon Power Amplifiers and Transmitters* (The Cambridge RF and Microwave Engineering Series). Cambridge, U.K.: Cambridge Univ. Press, 2016. [Online]. Available: https://books.google.co.uk/books?id=hUbGCwAAQBAJ

[41] B. Evans, M. Werner, E. Lutz, M. Bousquet, G. E. Corazza, and G. Maral, "Integration of satellite and terrestrial systems in future multimedia communications," *IEEE Wireless Commun.*, vol. 12, no. 5, pp. 72–80, Oct. 2005.

[42] X. Li, A. Gani, R. Salleh, and O. Zakaria, "The future of mobile wireless communication networks," in *Proc. IEEE Int. Conf. Commun. Softw. Netw. (ICCSN)*, 2009, pp. 554–557, doi: 10.1109/ICCSN.2009.105.

[43] T. L. Marzetta, "Fundamental limitations on the capacity of wireless links that use polarimetric antenna arrays," in *Proc. IEEE Int. Symp. Inf. Theory*, Jun./Jul. 2002, p. 51, doi: 10.1109/ISIT.2002.1023323.

[44] T. Svantesson, M. A. Jensen, and J. W. Wallace, "Analysis of electromagnetic field polarizations in multiantenna systems," *IEEE Trans. Wireless Commun.*, vol. 3, no. 2, pp. 641–646, Mar. 2004.

[45] J. W. Wallace and M. A. Jensen, "Mutual coupling in MIMO wireless systems: A rigorous network theory analysis," *IEEE Trans. Wireless Commun.*, vol. 3, no. 4, pp. 1317–1325, Jul. 2004.

[46] C. Y. Chiu, C. H. Cheng, R. D. Murch, and C. R. Rowell, "Reduction of mutual coupling between closely-packed antenna elements," *IEEE Trans. Antennas Propag.*, vol. 55, no. 6, pp. 1732–1738, Jun. 2007.

[47] Y. Gao, S. Wang, O. Falade, X. Chen, C. Parini, and L. Cuthbert, "Mutual coupling effects on pattern diversity antennas for MIMO femtocells," *Int. J. Antennas Propag.*, vol. 2010, Apr. 2010, Art. no. 756848, doi: 10.1155/2010/756848.

[48] A. Diallo, C. Luxey, P. Le Thuc, R. Staraj, and G. Kossiavas, "Study and reduction of the mutual coupling between two mobile phone PIFAs operating in the DCS1800 and UMTS bands," *IEEE Trans. Antennas Propag.*, vol. 54, no. 11, pp. 3063–3074, Nov. 2006.

[49] S. L. S. Yang, K. M. Luk, H. W. Lai, A. A. Kishk, and K. F. Lee, "A dual-polarized antenna with pattern diversity," *IEEE Antennas Propag. Mag.*, vol. 50, no. 6, pp. 71–79, Dec. 2008.

[50] A. Chebihi, C. Luxey, A. Diallo, P. L. Thuc, and R. Staraj, "A novel isolation technique for closely spaced PIFAs for UMTS mobile phones," *IEEE Antennas Wireless Propag. Lett.*, vol. 7, pp. 665–668, 2008.

[51] M. C. Mtumbuka and D. J. Edwards, "Investigation of tri-polarised MIMO technique," *Electron. Lett.*, vol. 41, no. 3, pp. 137–138, Feb. 2005.

[52] M. C. Mtumbuka, W. Q. Malik, C. J. Stevens, and D. J. Edwards, "A tri-polarized ultra-wideband MIMO system," in *Proc. IEEE Symp. Adv. Wired Wireless Commun.*, Apr. 2005, pp. 98–101, doi: 10.1109/SARNOF.2005.1426521.

[53] L. C. Lukama, K. Konstantinou, and D. J. Edwards, "Performance of a three-branch orthogonal polarization diversity scheme," in *Proc. IEEE 54th Veh. Technol. Conf. (VTC)-Fall*, Oct. 2001, pp. 2033–2037, doi: 10.1109/VTC.2001.957101.

[54] B. N. Getu and J. B. Andersen, "The MIMO cube—A compact MIMO antenna," *IEEE Trans. Wireless Commun.*, vol. 4, no. 3, pp. 1136–1141, May 2005.

[55] B. N. Getu and R. Janaswamy, "The effect of mutual coupling on the capacity of the MIMO cube," *IEEE Antennas Wireless Propag. Lett.*, vol. 4, pp. 240–244, 2005.

[56] J. X. Yun and R. G. Vaughan, "Slot MIMO cube," in *Proc. IEEE Antennas Propag. Soc. Int. Symp. (APSURSI)*, Jul. 2010, pp. 1–4, doi: 10.1109/APS.2010.5560947.

[57] L. Zou and C. Fumeaux, "A cross-shaped dielectric resonator antenna for multifunction and polarization diversity applications," *IEEE Antennas Wireless Propag. Lett.*, vol. 10, pp. 742–745, 2011.

[58] D. Gesbert, M. Shafi, D. Shiu, P. J. Smith, and A. Naguib, "From theory to practice: An overview of MIMO space-time coded wireless systems," *IEEE J. Sel. Areas Commun.*, vol. 21, no. 3, pp. 281–302, Apr. 2003.

[59] A. M. Tulino, A. Lozano, and S. Verdu, "Impact of antenna correlation on the capacity of multiantenna channels," *IEEE Trans. Inf. Theory*, vol. 51, no. 7, pp. 2491–2509, Jul. 2005.

[60] N. P. Lawrence, H. J. Hansen, and D. Abbott, "Tri-orthogonal polarization diversity reception for non-geosynchronous satellite orbit ionospheric channels," *Int. J. Satellite Commun. Netw.*, to be published. [Online]. Available: http://dx.doi.org/10.1002/sat.1203, doi: 10.1002/sat.1203.

[61] R. U. Nabar, H. Bolcskei, V. Erceg, D. Gesbert, and A. J. Paulraj, "Performance of multiantenna signaling techniques in the presence of polarization diversity," *IEEE Trans. Signal Process.*, vol. 50, no. 10, pp. 2553–2562, Oct. 2002.

[62] V. Eiceg, H. Sampath, and S. Catreux-Erceg, "Dual-polarization versus single-polarization MIMO channel measurement results and modeling," *IEEE Trans. Wireless Commun.*, vol. 5, no. 1, pp. 28–33, Jan. 2006.

[63] M. Coldrey, "Modeling and capacity of polarized MIMO channels," in *Proc. IEEE Veh. Technol. Conf. (VTC)-Spring*, May 2008, pp. 440–444, doi: 10.1109/VETECS.2008.103.

[64] P.-D. Arapoglou, K. Liolis, M. Bertinelli, A. Panagopoulos, P. Cottis, and R. De Gaudenzi, "MIMO over satellite: A review," *IEEE Commun. Surveys Tuts.*, vol. 13, no. 1, pp. 27–51, 1st Quart., 2011.

[65] P.-D. Arapoglou, P. Burzigotti, A. B. Alamañac, and R. D. Gaudenzi, "Practical MIMO aspects in dual polarization per beam mobile satellite broadcasting," *Int. J. Satellite Commun. Netw.*, vol. 30, no. 2, pp. 76–87, 2012. [Online]. Available: http://dx.doi.org/10.1002/sat.1008, doi: 10.1002/sat.1008.

[66] M. Shafi *et al.*, "Polarized MIMO channels in 3-D: Models, measurements and mutual information," *IEEE J. Sel. Areas Commun.*, vol. 24, no. 3, pp. 514–527, Mar. 2006.

[67] S. C. Kwon and G. L. Stüber, "Geometrical theory of channel depolarization," *IEEE Trans. Veh. Technol.*, vol. 60, no. 8, pp. 3542–3556, Oct. 2011.

[68] M. T. Dao, V. A. Nguyen, Y. T. Im, S. O. Park, and G. Yoon, "3D polarized channel modeling and performance comparison of MIMO antenna configurations with different polarizations," *IEEE Trans. Antennas Propag.*, vol. 59, no. 7, pp. 2672–2682, Jul. 2011.

[69] R. Compton, Jr., "The tripole antenna: An adaptive array with full polarization flexibility," *IEEE Trans. Antennas Propag.*, vol. 29, no. 6, pp. 944–952, Nov. 1981.

[70] G. Gupta, B. L. Hughes, and G. Lazzi, "On the degrees of freedom in linear array systems with tri-polarized antennas," *IEEE Trans. Wireless Commun.*, vol. 7, no. 7, pp. 2458–2462, Jul. 2008.

[71] F. Quitin, C. Oestges, F. Horlin, and P. D. Doncker, "Multipolarized MIMO channel characteristics: Analytical study and experimental results," *IEEE Trans. Antennas Propag.*, vol. 57, no. 9, pp. 2739–2745, Sep. 2009.

[72] D. Piao, L. Yang, Q. Guo, Y. Mao, and Z. Li, "Measurement-based performance comparison of colocated tripolarized loop and dipole antennas," *IEEE Trans. Antennas Propag.*, vol. 63, no. 8, pp. 3371–3379, Aug. 2015.

[73] L. Coetzee and J. Eksteen, "The Internet of Things—Promise for the future? An introduction," in *Proc. IST-Africa Conf.*, May 2011, pp. 1–9. [Online]. Available: http://ieeexplore.ieee.org/stamp/stamp.jsp?arnumber=6107386

[74] J. B. Kenney, "Dedicated short-range communications (DSRC) standards in the United States," *Proc. IEEE*, vol. 99, no. 7, pp. 1162–1182, Jul. 2011.

[75] S. Biswas, R. Tatchikou, and F. Dion, "Vehicle-to-vehicle wireless communication protocols for enhancing highway traffic safety," *IEEE Commun. Mag.*, vol. 44, no. 1, pp. 74–82, Jan. 2006.

[76] W. J. Jakes, Ed., *Microwave Mobile Communications*. New York, NY, USA: Wiley, 1974.

[77] T. S. Rappaport, *Wireless Communications: Principles and Practice*, 2nd ed. Englewood Cliffs, NJ, USA: Prentice-Hall, 1996.

[78] A. Paulraj, D. A. Gore, R. U. Nabar, and H. Bolcskei, "An overview of MIMO communications—A key to gigabit wireless," *Proc. IEEE*, vol. 92, no. 2, pp. 198–218, Feb. 2004.

[79] G. J. Foschini and M. J. Gans, "On limits of wireless communications in a fading environment when using multiple antennas," *Wireless Pers. Commun.*, vol. 6, no. 3, pp. 311–335, Mar. 1998. [Online]. Available: http://dx.doi.org/10.1023/A:1008889222784

[80] İ. E. Telatar, "Capacity of multi-antenna Gaussian channels," *Eur. Trans. Telecommun.*, vol. 10, no. 6, pp. 585–595, 1999. [Online]. Available: http://dx.doi.org/10.1002/ett.4460100604

[81] D.-S. Shiu, G. J. Foschini, M. J. Gans, and J. M. Kahn, "Fading correlation and its effect on the capacity of multielement antenna systems," *IEEE Trans. Commun.*, vol. 48, no. 3, pp. 502–513, Mar. 2000.

[82] J.-P. Kermoal, L. Schumacher, K. I. Pedersen, P. E. Mogensen, and F. Frederiksen, "A stochastic MIMO radio channel model with experimental validation," *IEEE J. Sel. Areas Commun.*, vol. 20, no. 6, pp. 1211–1226, Aug. 2002.

[83] C.-N. Chuah, D. N. C. Tse, J. M. Kahn, and R. A. Valenzuela, "Capacity scaling in MIMO wireless systems under correlated fading," *IEEE Trans. Inf. Theory*, vol. 48, no. 3, pp. 637–650, Mar. 2002.

[84] S. Kozono, T. Tsuruhara, and M. Sakamoto, "Base station polarization diversity reception for mobile radio," *IEEE Trans. Veh. Technol.*, vol. 33, no. 4, pp. 301–306, Nov. 1984.

[85] D. C. Cox, "Antenna diversity performance in mitigating the effects of portable radiotelephone orientation and multipath propagation," *IEEE Trans. Commun.*, vol. 31, no. 5, pp. 620–628, May 1983.

[86] D. C. Cox, R. R. Murray, H. W. Arnold, A. Norris, and M. Wazowicz, "Cross-polarization coupling measured for 800 MHz radio transmission in and around houses and large buildings," *IEEE Trans. Antennas Propag.*, vol. 34, no. 1, pp. 83–87, Jan. 1986.

[87] C. B. Dietrich, K. Dietze, J. R. Nealy, and W. L. Stutzman, "Spatial, polarization, and pattern diversity for wireless handheld terminals," *IEEE Trans. Antennas Propag.*, vol. 49, no. 9, pp. 1271–1281, Sep. 2001.

[88] R. R. Ramirez and F. D. Flaviis, "A mutual coupling study of linear and circular polarized microstrip antennas for diversity wireless systems," *IEEE Trans. Antennas Propag.*, vol. 51, no. 2, pp. 238–248, Feb. 2003.

[89] P. Kyritsi, D. C. Cox, R. A. Valenzuela, and P. W. Wolniansky, "Effect of antenna polarization on the capacity of a multiple element system in an indoor environment," *IEEE J. Sel. Areas Commun.*, vol. 20, no. 6, pp. 1227–1239, Aug. 2002.

[90] V. Erceg, P. Soma, D. S. Baum, and S. Catreux, "Multiple-input multiple-output fixed wireless radio channel measurements and modeling using dual-polarized antennas at 2.5 GHz," *IEEE Trans. Wireless Commun.*, vol. 3, no. 6, pp. 2288–2298, Nov. 2004.

[91] C. Oestges, B. Clerckx, M. Guillaud, and M. Debbah, "Dual-polarized wireless communications: From propagation models to system performance evaluation," *IEEE Trans. Wireless Commun.*, vol. 7, no. 10, pp. 4019–4031, Oct. 2008.

[92] V. Degli-Esposti, V.-M. Kolmonen, E. M. Vitucci, and P. Vainikainen, "Analysis and modeling on co- and cross-polarized urban radio propagation for dual-polarized MIMO wireless systems," *IEEE Trans. Antennas Propag.*, vol. 59, no. 11, pp. 4247–4256, Nov. 2011.

[93] T. Kleine-Ostmann and T. Nagatsuma, "A review on terahertz communications research," *J. Infr., Millim. Terahertz Waves*, vol. 32, no. 2, pp. 143–171, 2011.

[94] C. Fumeaux *et al.*, "Terahertz and optical dielectric resonator antennas: Potential and challenges for efficient designs," in *Proc. 10th Eur. Conf. Antennas Propag. (EuCAP)*, Apr. 2016, pp. 1–4.

[95] D. Headland, W. Withayachumnankul, M. Webb, and D. Abbott, "Beam deflection lens at terahertz frequencies using a hole lattice metamaterial," in *Proc. 38th Int. Conf. Infr., Millim., Terahertz Waves (IRMMW-THz)*, Sep. 2013, pp. 1–2.

[96] D. Turchinovich, A. Kammoun, P. Knobloch, T. Dobbertin, and M. Koch, "Flexible all-plastic mirrors for the THz range," *Appl. Phys. A*, vol. 74, no. 2, pp. 291–293, 2002.

[97] H. Guo, B. Luo, Y. Ren, S. Zhao, and A. Dang, "Influence of beam wander on uplink of ground-to-satellite laser communication and optimization for transmitter beam radius," *Opt. Lett.*, vol. 35, no. 12, pp. 1977–1979, Jun. 2010. [Online]. Available: http://ol.osa.org/abstract.cfm?URI=ol-35-12-1977

[98] M. Jacob, P. Herrero, and J. Schoebel, "Low-cost omnidirectional planar antennas for the 122 GHz ISM frequency band," in *Proc. IEEE Antennas Propag. Soc. Int. Symp.*, Jul. 2008, pp. 1–4, doi: 10.1109/APS.2008.4619478.

[99] R. C. Daniels and R. W. Heath, "60 GHz wireless communications: Emerging requirements and design recommendations," *IEEE Veh. Technol. Mag.*, vol. 2, no. 3, pp. 41–50, Sep. 2007.

[100] R. G. Vaughan, "Polarization diversity in mobile communications," *IEEE Trans. Veh. Technol.*, vol. 39, no. 3, pp. 177–186, Aug. 1990.
[101] K. P. Liolis, J. Gomez-Vilardebo, E. Casini, and A. I. Perez-Neira, "Statistical modeling of dual-polarized MIMO land mobile satellite channels," *IEEE Trans. Commun.*, vol. 58, no. 11, pp. 3077–3083, Nov. 2010.
[102] J. F. Valenzuela-Valdes, M. A. Garcia-Fernandez, A. M. Martinez-Gonzalez, and D. A. Sanchez-Hernandez, "Evaluation of true polarization diversity for MIMO systems," *IEEE Trans. Antennas Propag.*, vol. 57, no. 9, pp. 2746–2755, Sep. 2009.
[103] A. Farkasvolgyi, R. Dady, and L. Nagy, "Channel capacity maximization in MIMO antenna system by genetic algorithm," in *Proc. 3rd Eur. Conf. Antennas Propag. (EuCAP)*, 2009, pp. 1119–1122. [Online]. Available: http://ieeexplore.ieee.org/stamp/stamp.jsp?tp=&arnumber=5067812?
[104] J. F. Valenzuela-Valdes and D. A. Sanchez-Hernandez, "Increasing handset performance using true polarization diversity," in *Proc. IEEE 69th Veh. Technol. Conf. (VTC)-Spring*, Apr. 2009, pp. 1–4, doi: 10.1109/VETECS.2009.5073600.
[105] G. R. Fowles, *Introduction to Modern Optics*, 2nd ed. New York, NY, USA: Dover, 1989.
[106] M. Jehle, M. Rüegg, D. Small, E. Meier, and D. Nüesch, "Estimation of ionospheric TEC and Faraday rotation for L-band SAR," *Proc. SPIE*, vol. 5979, pp. 252–260, Oct. 2005.
[107] N. P. Lawrence, B. W.-H. Ng, H. J. Hansen, and D. Abbott, "Analysis of millimetre-wave polarization diverse multiple-input multiple-output capacity," *Roy. Soc. Open Sci.*, vol. 2, no. 12, p. 150322, 2015. [Online]. Available: http://rsos.royalsocietypublishing.org/content/2/12/150322, doi: 10.1098/rsos.150322.
[108] P. Horváth and I. Frigyes, "SAT02-6: Application of the 3D polarization concept in satellite MIMO systems," in *Proc. IEEE Global Commun. Conf. (GlobeCom)*, Nov./Dec. 2006, pp. 1–5, doi: 10.1109/GLOCOM.2006.481.
[109] S. Sirianunpiboon, S. D. Howard, A. R. Calderbank, and L. M. Davis, "Fully-polarimetric MIMO to improve throughput and reliability across propagation conditions," in *Proc. IEEE 70th Veh. Technol. Conf. (VTC)-Fall*, Sep. 2009, pp. 1–5, doi: 10.1109/VETECF.2009.5379016.
[110] J. G. Proakis, *Digital Communications*. New York, NY, USA: McGraw-Hill, 2001.
[111] A. Paulraj, R. Nabar, and D. Gore, *Introduction to Space-Time Wireless Communications*. Cambridge, U.K.: Cambridge Univ. Press, 2003.
[112] J. Wang, H. Zhang, L. Tingting, and T. A. Gulliver, "Capacity of 60 GHz wireless communication systems over fading channels," *J. Netw.*, vol. 7, no. 1, pp. 203–209, 2012.
[113] L. Atzori, A. Iera, and G. Morabito, "The Internet of Things: A survey," *Comput. Netw.*, vol. 54, no. 15, pp. 2787–2805, Oct. 2010. [Online]. Available: http://www.sciencedirect.com/science/article/pii/S1389128610001568
[114] M. Keskilammi, L. Sydänheimo, and M. Kivikoski, "Radio frequency technology for automated manufacturing and logistics control. Part 1: Passive RFID systems and the effects of antenna parameters on operational distance," *Int. J. Adv. Manuf. Technol.*, vol. 21, no. 10, pp. 769–774, 2003. [Online]. Available: http://dx.doi.org/10.1007/s00170-002-1392-1
[115] P.-D. Arapoglou, P. Burzigotti, A. B. Alamanac, and R. De Gaudenzi, "Capacity potential of mobile satellite broadcasting systems employing dual polarization per beam," in *Proc. Adv. Satellite Multimedia Syst. Conf. (ASMA) Signal Process. Space Commun. Workshop (SPSC)*, Sep. 2010, pp. 213–220, doi: 10.1109/ASMS-SPSC.2010.5586911.
[116] P.-D. Arapoglou, M. Zamkotsian, and P. Cottis, "Dual polarization MIMO in LMS broadcasting systems: Possible benefits and challenges," *Int. J. Satellite Commun. Netw.*, vol. 29, no. 4, pp. 349–366, 2010. [Online]. Available: http://dx.doi.org/10.1002/sat.986, doi: 10.1002/sat.986.
[117] E. G. Larsson, O. Edfors, F. Tufvesson, and T. L. Marzetta, "Massive MIMO for next generation wireless systems," *IEEE Commun. Mag.*, vol. 52, no. 2, pp. 186–195, Feb. 2014.
[118] V. Erceg, P. Soma, D. S. Baum, and A. J. Paulraj, "Capacity obtained from multiple-input multiple-output channel measurements in fixed wireless environments at 2.5 GHz," in *Proc. IEEE Int. Conf. Commun.*, Apr./May 2002, pp. 396–400, doi: 10.1109/ICC.2002.996883.
[119] H. T. Friis, "A note on a simple transmission formula," *Proc. IRE*, vol. 34, no. 5, pp. 254–256, May 1946.
[120] S. J. Orfanidis, *Electromagnetic Waves and Antennas*. New Brunswick, NJ, USA: Rutgers Univ., 2002. [Online]. Available: http://www.ece.rutgers.edu/faculty/orfanidis
[121] N. Lawrence, L. M. Davis, and D. Haley, "A polarimetric line-of-sight channel model for MIMO satellite communications," in *Proc. IEEE Austral. Commun. Theory Workshop (AusCTW)*, Jan./Feb. 2013, pp. 99–104, doi: 10.1109/AusCTW.2013.6510052.
[122] N. P. Lawrence, C. Fumeaux, and D. Abbott, "Planar triorthogonal diversity slot antenna," *IEEE Trans. Antennas Propag.*, vol. 65, no. 3, pp. 1416–1421, Mar. 2017, doi: 10.1109/TAP.2016.2647719.
[123] N. P. Lawrence, C. Fumeaux, and D. Abbott, "Planar slot antenna with circular and vertical polarization diversity," *Electron. Lett.*, to be published.
[124] F. Bohagen, P. Orten, and G. E. Oien, "Construction and capacity analysis of high-rank line-of-sight MIMO channels," in *Proc. IEEE Wireless Commun. Netw. Conf.*, Mar. 2005, pp. 432–437, doi: 10.1109/WCNC.2005.1424539.
[125] V. R. Anreddy and M. A. Ingram, "Capacity of measured Ricean and Rayleigh indoor MIMO channels at 2.4 GHz with polarization and spatial diversity," in *Proc. IEEE Wireless Commun. Netw. Conf.*, Apr. 2006, pp. 946–951, doi: 10.1109/WCNC.2006.1683597.
[126] M.-S. Choi, G. Grosskopf, and D. Rohde, "Statistical characteristics of 60 GHz wideband indoor propagation channel," in *Proc. IEEE 16th Int. Symp. Pers., Indoor Mobile Radio Commun. (PIMRC)*, Sep. 2005, pp. 599–603, doi: 10.1109/PIMRC.2005.1651506.
[127] N. P. Lawrence, H. Hansen, and D. Abbott, "Tri-orthogonal polarization diversity for 5G networks," *Trans. Emerg. Telecommun. Technol.*, vol. 27, no. 7, pp. 992–999, 2016, doi: 10.1002/ett.3042.
[128] Nanjing University. *Waves in What?* accessed on 2016. [Online]. Available: http://astronomy.nju.edu.cn/~lixd/GA/AT4/AT403/HTML/AT40302.htm

NICHOLAS P. LAWRENCE was born in Chichester, U.K., in 1972. He received the B.Sc. degree (Hons) in physics from the University of Leicester, U.K., in 1995, and the M.Sc. degree (Hons.) in microwave solid state physics from the University of Portsmouth, U.K. in 1997, the M.Phil. degree in fiber optic sensing techniques from the University of Southampton, U.K. in 2002. He is currently pursuing the Ph.D. degree with The University of Adelaide, Australia, under the supervision of H. Hansen and D. Abbott, with a focus on applications of MIMO polarimetry in remote sensing and communication. Since 2002, he has been a Radio Frequency Power Amplifier Engineer specializing in linearity techniques employed in applications ranging from high-power military applications to commercial COFDM broadcast systems. He is currently a Chartered Engineer with the Institute of Engineering and Technology, U.K., since 2004.

BRIAN WAI-HIM NG (S'97–M'02) was born in Hong Kong in 1974. He received the B.Sc. degree in mathematics and computer science, and the B.Eng. degree (Hons) and the Ph.D. degree in electrical and electronic engineering, under A. Bouzerdoum, from The University of Adelaide, Australia, in 1996, 1997, and 2003, respectively. He is currently a Senior Lecturer with the School of Electrical and Electronic Engineering, The University of Adelaide. His research interests include radar signal processing, wavelets and terahertz (T-ray) signal processing. He was a recipient of The University of Adelaide Medal for the Top Graduate in Electrical and Electronic Engineering. He is currently an active member within the South Australian Chapter of the IEEE.

HEDLEY J. HANSEN (M'98) was born in Port Elizabeth, South Africa, in 1957. He received the B.Sc. (Hons), M.Sc. *(cum laude)*, and Ph.D. degrees from the University of Natal, Durban, South Africa, in 1980, 1983, and 1988, respectively. His Ph.D. research was concerned with the magnetospheric wave particle interaction processes that give rise to the optical aurora, under the supervision of Malcolm W. J. Scourfield. In 1988, he joined the Space Plasma Waves Group, The University of Newcastle, NSW, Australia, as a Post-doctoral Research Associate. The group maintained arrays of induction magnetometers in Australian Antarctic Territory and across the Australian Mainland. He moved to the RF Technology Group, Electronic Warfare, and Radar Division, Defense Science and Technology Organization, Edinburgh, South Australia, in 1996, as a Senior Research Scientist. He is currently an adjunct Senior Lecturer with The University of Adelaide. His professional interests lie in RF remote sensing at millimeter and submillimeter wavelengths, in microstrip antenna design, and in phased array, and miniaturized radar technologies. He is a member of the American Geophysical Union and the Australian Institute of Physics. He currently chairs the AP&MTT Chapter (South Australian section) of the IEEE.

DEREK ABBOTT (M'85–SM'99–F'05) was born in South Kensington, London, U.K., in 1960. He received the B.Sc. (Hons.) degree in physics from Loughborough University, U.K., in 1982, and the Ph.D. degree in electrical and electronic engineering from The University of Adelaide, Australia, in 1995, under the supervision of K. Eshraghian and B. R. Davis. From 1978 to 1986, he was a Research Engineer with the GEC Hirst Research Center, London. From 1986 to 1987, he was a VLSI Design Engineer with Austek Microsystems, Australia. Since 1987, he has been with The University of Adelaide, where he is currently a Full Professor with the School of Electrical and Electronic Engineering. He holds over 800 publications and has been an Invited Speaker at over 100 institutions. He has co-edited *Quantum Aspects of Life* (Imperial College Press), co-authored *Stochastic Resonance* (Cambridge University Press), and *Terahertz Imaging for Biomedical Applications* (Springer-Verlag). His interests are in the area of multidisciplinary physics and electronic engineering applied to complex systems and frequencies up to the terahertz range. He is a fellow of the Institute of Physics (IOP). He has received a number of awards, including the South Australian Tall Poppy Award for Science in 2004, the Premier's SA Great Award in Science and Technology for Outstanding Contributions to South Australia in 2004, the Australian Research Council Future Fellowship in 2012, and the David Dewhurst Medal in 2015. He is currently on the editorial boards of the Nature's Scientific Reports, the IEEE Access, and the Royal Society Open Science. He has served as an Editor and/or Guest Editor of a number of journals, including the IEEE JOURNAL OF SOLID-STATE CIRCUITS, the *Journal of Optics B* (IOP), *Microelectronics Journal* (Elsevier), *Chaos* (AIP), *Smart Structures and Materials* (IOP), *Fluctuation Noise Letters* (World Scientific), PLoS ONE, PROCEEDINGS of the IEEE, and the IEEE PHOTONICS JOURNAL.